Monthly Notices of the ROYAL ASTRONOMICAL SOCIETY

MNRAS **526,** 4209–4233 (2023) https://doi.org/10.1093/mnras/stad3005
Advance Access publication 2023 October 05

Volatiles in the H_2O and CO_2 ices of comet 67P/Churyumov–Gerasimenko

Martin Rubin [1]★ Kathrin Altwegg [1] Jean-Jacques Berthelier [2] Michael R. Combi [3] Johan De Keyser [4] Stephen A. Fuselier [5,6] Tamas I. Gombosi [3] Murthy S. Gudipati [7] Nora Hänni [1] Kristina A. Kipfer [1,8] Niels F. W. Ligterink [1] Daniel R. Müller [1] Yinsi Shou [3] and Susanne F. Wampfler [9]

[1]*Space Research and Planetary Sciences, Physics Institute, University of Bern, Sidlerstrasse 5, CH-3012 Bern, Switzerland*
[2]*Laboratoire Atmosphéres, Milieux, Observations Spatiales, Institut Pierre Simon Laplace, CNRS, Université Pierre et Marie Curie, 4 Avenue de Neptune, F-94100 Saint-Maur, France*
[3]*Department of Climate and Space Sciences and Engineering, University of Michigan, 2455 Hayward, Ann Arbor, MI 48109, USA*
[4]*Royal Belgian Institute for Space Aeronomy, BIRA-IASB, Ringlaan 3, B-1180 Brussels, Belgium*
[5]*Space Science Directorate, Southwest Research Institute, 6220 Culebra Rd., San Antonio, TX 78228, USA*
[6]*Department of Physics and Astronomy, The University of Texas at San Antonio, San Antonio, TX 78249, USA*
[7]*Science Division, Jet Propulsion Laboratory, California Institute of Technology, 4800 Oak Grove Drive, Pasadena, CA 91109, USA*
[8]*NCCR PlanetS, Gesellschaftsstrasse 6, CH-3012 Bern, Switzerland*
[9]*Center for Space and Habitability, University of Bern, Gesellschaftsstrasse 6, CH-3012 Bern, Switzerland*

Accepted 2023 October 2. Received 2023 September 27; in original form 2023 August 30

ABSTRACT

European Space Agency's Rosetta spacecraft at comet 67P/Churyumov–Gerasimenko (67P) was the first mission that accompanied a comet over a substantial fraction of its orbit. On board was the Rosetta Orbiter Spectrometer for Ion and Neutral Analysis mass spectrometer suite to measure the local densities of the volatile species sublimating from the ices inside the comet's nucleus. Understanding the nature of these ices was a key goal of Rosetta. We analysed the primary cometary molecules at 67P, namely H_2O and CO_2, together with a suite of minor species for almost the entire mission. Our investigation reveals that the local abundances of highly volatile species, such as CH_4 and CO, are reproduced by a linear combination of both H_2O and CO_2 densities. These findings bear similarities to laboratory-based temperature-programmed desorption experiments of amorphous ices and imply that highly volatile species are trapped in H_2O and CO_2 ices. Our results do not show the presence of ices dominated by these highly volatile molecules. Most likely, they were lost due to thermal processing of 67P's interior prior to its deflection to the inner solar system. Deviations in the proportions co-released with H_2O and CO_2 can only be observed before the inbound equinox, when the comet was still far from the sun and the abundance of highly volatile molecules associated with CO_2 outgassing were lower. The corresponding CO_2 is likely seasonal frost, which sublimated and lost its trapped highly volatile species before re-freezing during the previous apparition. CO, on the other hand, was elevated during the same time and requires further investigation.

Key words: comets: general – comets: individual: 67P/Churyumov-Gerasimenko.

1 INTRODUCTION

Comets are remnants of the formation of our solar system (Weissman et al. 2020). As they spend their lifetime predominantly far away from the sun, they belong to the most pristine objects in the solar system. Due to this, observing comets reveals key information about the initial composition of the protoplanetary disc. To date, numerous comets have been observed remotely or have even been visited by spacecraft. The extensive body of cometary coma observations revealed a plethora of volatile species which originate from sublimation of ices inside their nuclei, on their surfaces, or from icy grains in the dust coma (see e.g. A'Hearn et al. 2011). The most abundant molecules are water (H_2O), carbon dioxide (CO_2) and carbon monxide (CO), cf. A'Hearn et al. (2012) and Biver & Bockelée-Morvan (2019). Also a suite of minor volatiles have been observed, these include methane (CH_4), ethane (C_2H_6), propane (C_3H_8), molecular oxygen (O_2) and methanol (CH_3OH) among many others (Bockelée-Morvan et al. 2004; Bieler et al. 2015; Dello Russo et al. 2016; Schuhmann et al. 2019; Rubin et al. 2020). All these volatile species cover a wide range in sublimation temperatures, from about 20 K to the sublimation of water at around 140 K (Fray & Schmitt 2009).

Given that the vast majority of the relative abundances of these species have been derived from measurements of the gaseous coma surrounding the nucleus and mostly during the most active phase near perihelion, important questions remain unanswered. For instance, how are these volatiles stored in cometary ices inside the nucleus? There are several concurrent theories and the debate is still ongoing. Cometary ices may have formed through freeze out in the protosolar

★ E-mail: martin.rubin@unibe.ch

nebula (PSN) with possible trapping of minor species in clathrates (Luspay-Kuti et al. 2016). The other possibility is the inheritance of amorphous cometary ices from stages prior to the formation of the solar system, e.g, from the prestellar core stage or interstellar medium (ISM), before incorporation into the nucleus (Altwegg et al. 2017a). Both scenarios have been investigated extensively using numerical models and, where possible, with laboratory measurements (Bar-Nun, Notesco & Owen 2007; Laufer, Bar-Nun & Ninio Greenberg 2017; Mousis et al. 2018). Still, the debate remains to be settled. In particular because direct observations of pristine cometary ices are very limited and most evidence is derived from measurements of the gases in the coma.

Between 2014–2016, the European Space Agency's (ESA) Rosetta mission followed comet 67P/Churyumov–Gerasimenko (hereafter 67P) for over 2 yr and carried out a close inspection of its nucleus and surrounding gas and dust coma (Taylor et al. 2017). Rosetta was designed to tackle a whole set of science goals, among them the determination of the composition of volatiles and the investigation of outgassing activity and associated seasonal effects (Glassmeier et al. 2007). Rosetta provided numerous new and surprising insights (Fulle et al. 2016), nevertheless, a number of questions remain in addition to new ones raised, in particular regarding activity and the origin and processing of the ices inside the comet's nucleus (Thomas et al. 2019).

Understanding cometary activity requires detailed knowledge of the composition of the outgassing layer near the surface of the nucleus. For this purpose, we analyse data from the Rosetta/ROSINA mass spectrometer suite (Rosetta Orbiter Spectrometer for Ion and Neutral Analysis; Balsiger et al. 2007) and then compare our results to the scenario of volatiles trapped in amorphous ice. In the following, we first introduce the Rosetta mission to comet 67P in Section 2. Afterwards, we review some of the findings from laboratory experiments in Section 3. The measurements obtained by Rosetta follow in Section 4 and a discussion with regards to the trapping of volatiles follows in Section 5. A summary of the major findings in Section 6 concludes the paper.

2 ROSETTA MISSION

The Rosetta mission was launched on 2004 March 2 from Kourou, French Guayana, and arrived at comet 67P in early 2014 August. For the next 25 months, Rosetta followed the comet along its orbit around the sun and carried out an in-depth investigation of its nucleus and surrounding gas, dust, and plasma environment (Taylor et al. 2017). During that time, 67P covered a heliocentric distance from well beyond 3.5 au inbound, through perihelion at 1.24 au in 2015 August, and outbound to almost 4 au again. Rosetta remained within a few several tens to hundreds of kilometres from the nucleus for the majority of the mission, depending on the outgassing activity of the comet. A substantial fraction was spent in gravitationally bound orbits within 30 km from the nucleus and in the terminator plane. Combined with the comet's rotation, Rosetta covered the entire surface and repetitively passed over the same subspacecraft latitudes and longitudes which allowed to study the long-term evolution of the nucleus and its surroundings. The mission was terminated by the end of 2016 September, when the Rosetta spacecraft itself landed on the surface of the comet.

Among the payload instruments on the orbiter was ROSINA (Balsiger et al. 2007) which was dedicated to the *in situ* measurement of the major and minor volatile species at the location of the spacecraft (Altwegg, Balsiger & Fuselier 2019). In the following, key aspects of the ROSINA instrument suite (Section 2.1) and the target, comet 67P (Section 2.2) are introduced.

2.1 The ROSINA instrument

The Double Focussing Mass Spectrometer (DFMS) and the COmet Pressure Sensor (COPS) were both part of the ROSINA instrument suite (Balsiger et al. 2007). DFMS was a mass spectrometer used to obtain the relative abundances of the volatile species at the location of Rosetta, in the coma of the comet. DFMS measured sequentially around each integer mass-per-charge ratio. Hence, the different volatile species in the coma were not acquired at the same time, for example, there was a time difference of 13 min between the major coma species H_2O and CO_2. Therefore, the measured signals of a given species were linearly interpolated in time and normalized to the water signal to obtain relative abundances. Afterwards, the absolute densities were derived by scaling to the total density measured by COPS while maintaining the above-discussed relative abundances (Rubin et al. 2019b).

Both DFMS and COPS had large fields of view (FoV), which most of the time, due to the cometocentric distance of Rosetta, covered much more than the entire nucleus of 67P. Thus, it is not possible to pinpoint the exact origin of the molecules measured by ROSINA on the nucleus itself, but at least an approximate location can be identified (Combi et al. 2020; Läuter et al. 2020). In this work, however, we focus on the analysis of the local gas measurements at Rosetta instead of the source distribution on the nucleus.

More details about ROSINA DFMS and COPS and the data treatment can be found in Appendix A.

2.2 Comet 67P

Comet 67P, a Jupiter-family Comet (JFC) on its current orbit since a close encounter with Jupiter in 1959 (Maquet 2015), has an orbital period of 6.4 yr and a perihelion distance of ∼1.24 au. The comet has a pronounced bi-lobate shape (Sierks et al. 2015) and a rotation period that dropped from 12.4 to 12.0 h during the inbound phase due to torques induced by outgassing, mostly during the peak activity period around perihelion (Kramer et al. 2019). Comet 67P's highly irregular shape most likely resulted from a collisional merger of two cometesimals (Jutzi & Asphaug 2015; Massironi et al. 2015). The physical dimensions are approximately 4 km along the long axis and roughly 2–3 km in perpendicular direction. This, combined with the obliquity of 67P's rotation axis of 52° (Sierks et al. 2015), leads to pronounced seasonal outgassing (Hässig et al. 2015). Summer on the Northern hemisphere lasts for more than 5 yr and covers the portion of the orbit away from the sun. The Southern hemisphere, on the other hand, exhibits a short but intense summer lasting less than 1 yr and includes perihelion. As a result, most of the gas and dust activity and hence also erosion occurs on the Southern hemisphere (Keller et al. 2015, 2017).

A number of neutral gas species' local and column densities have been monitored throughout the Rosetta mission by a suite of instruments. This includes Rosetta/MIRO (Microwave Instrument on the Rosetta Orbiter, Marshall et al. 2017; Biver et al. 2019), Rosetta/VIRTIS (Visual IR Thermal Imaging Spectrometer, Bockelée-Morvan et al. 2015, 2016), and Rosetta/ROSINA (Rubin et al. 2019a; Läuter et al. 2020) as well as multi-instrument studies including Rosetta/RPC (Rosetta Plasma Consortium), the Japanese PROCYON/LAICA (Proximate Object Close Flyby with Optical Navigation/Lyman-Alpha Imaging Camera) wide-field imager, and ground-based observations of the dust activity (Hansen et al. 2016; Combi et al. 2020).

The major volatile species in 67P's coma are H_2O and CO_2. Additionally, CO, O_2, and H_2S (hydrogen sulfide) are present on the level of up to a few per cent by number with respect to water (Combi et al. 2020; Läuter et al. 2020). All the other volatile species' abundances are below the per cent level (Rubin et al. 2019b). No apparent difference in composition has been reported for the two lobes. Also the deuterium-to-hydrogen ratio in water, found to be elevated in comet 67P (Altwegg et al. 2015), was homogeneous within errors between both lobes (Schroeder et al. 2019). Strong compositional heterogeneity in the gas coma, however, was observed above the Northern versus the Southern hemisphere due to the aforementioned obliquity of the rotation axis and associated seasons and is hence most likely of evolutionary origin (Le Roy et al. 2015).

The complex shape and orientation of the spin axis results in not only a complicated seasonal but also diurnal outgassing cycle with strongly varying relative abundances of coma volatiles (Hässig et al. 2015; Le Roy et al. 2015). Depending on the location of the Rosetta spacecraft, combined with the orientation of the nucleus, the main volatile in the coma could either be H_2O or CO_2. Based on early mission data, Le Roy et al. (2015) showed that the relative gas abundances in the coma with respect to water changed substantially from the, at the time, illuminated Northern summer hemisphere to the Southern winter hemisphere. For instance, the CO_2/H_2O ratio changed by a factor $\sim$30, the CO/H_2O ratio by $\sim$7, the CH_4/H_2O ratio by $\sim$4, and the C_2H_6/H_2O ratio by $\sim$10. Hässig et al. (2015) suggested that these variations are governed by temperature variations, which depend on the depth of the outgassing layer and the changing illumination of the rotating nucleus.

Luspay-Kuti et al. (2015, 2019) studied correlations of different volatiles above the Southern hemisphere in- and outbound beyond 3 au. The analysis included HCN (hydrogen cyanide), CH_3OH, C_2H_6, CH_4, and CO in comparison to a mix of the primary volatiles H_2O and CO_2. In particular, CH_4 exhibited a distinct diurnal outgassing pattern which did no follow either of the major species. The authors could then attribute the pronounced changes in the abundances of these volatiles from pre- to post-equinox to seasonally driven heterogeneity of the nucleus caused by strong erosion of the Southern hemisphere.

Gasc et al. (2017) investigated a suite of eight species (H_2O, O_2, NH_3 (ammonia), H_2S, CH_4, HCN, CO_2, and CO) and showed that their outgassing pattern did not correlate with the sublimation temperature or polarity of the molecules. During the outbound journey, the different species' outgassing activity showed a dependence on the heliocentric distance between H_2O ($r_h^{-7.32\pm0.04}$) and CO_2 ($r_h^{-2.18\pm0.04}$). The authors interpreted this result to be the consequence of two different ice phases, H_2O and CO_2, with all the other species trapped in different relative abundances in these ices, consistent with the re-analysis of O_2 by Luspay-Kuti et al. (2022).

67P also exhibits a hemispherical dust transport across the surface due to inhomogeneous outgassing and dust activity (Rubin et al. 2014; Thomas et al. 2015). Such transport of material has also been observed at other comets, such as the redeposition of icy grains at comet 103P/Hartley 2 (A'Hearn et al. 2011). At 67P and in particular during the short but intense summer period around perihelion, substantial erosion occurs on the Southern hemisphere (Keller et al. 2015). Dust is lifted, transported and redeposited on the Northern hemisphere (Keller et al. 2017).

3 TEMPERATURE-PROGRAMMED DESORPTION EXPERIMENTS

Temperature-programmed desorption (TPD) measurements are an established laboratory technique to study the desorption processes of ices in the astrophysical context including comets (Burke & Brown 2010; Minissale et al. 2022). A number of relevant species have been co-deposited together with H_2O (e.g. Collings et al. 2004; Martín-Doménech et al. 2014; Almayrac et al. 2022) and CO_2 (e.g. Simon et al. 2019) at different trapping temperatures. The release of volatiles was then studied during a defined, most often linear, warm-up phase, hence the name of the technique. Key input parameters for such experiments include the gas composition, the temperature of the cold substrate on which the gas was frozen out, the thickness of the accumulated ice, and the heating rate used during the subsequently monitored desorption process (Collings et al. 2004).

In the programmed warm-up phase, species are released in different temperature regimes. For highly volatile molecules, like CH_4, CO, N_2 (molecular nitrogen), and O_2, a first part is released at or near its characteristic sublimation temperature (see e.g. Fray & Schmitt 2009). At elevated temperatures, the portion trapped in other species then co-desorbs at or near the sublimation temperature of the corresponding host species, for example, CO_2 and H_2O. In the following, we will refer to species with a pure ice sublimation temperature below that of CO_2 as highly volatile species.

Of particular interest for our work are the two most abundant species in comet 67P because they make up for the matrix/host phases: H_2O and CO_2 (Rubin et al. 2019b; Combi et al. 2020; Läuter et al. 2020). In the case of H_2O, the situation can be quite complex: trapped species are also released during the phase transition from low porosity amorphous to crystalline water ice, at lower temperatures than the main sublimation of water (Burke & Brown 2010). The release during the crystallization of amorphous water ice is also known as molecular volcano desorption (Smith et al. 1997). Additionally, whether a species is released entirely during the water ice phase transition or co-desorbs with H_2O also depends on the thickness of the ice: Notesco & Bar-Nun (2005) found that thin water ice films (0.1 μm) lose most trapped impurities, while thick water ices (5 μm) may quench the outward diffusion and the gas release then follows together with the main water ice sublimation. However, low levels of water desorption can occur before the amorphous to crystalline phase transition of water (Gudipati et al. 2023). This is of particular importance when ample time is available, as in the case of the ISM. In this situation, the bulk of the H_2O outgassing occurs already at much lower temperatures. The same applies to CO_2 and other volatiles (Ligterink & Minissale 2023).

TPD experiments are crucial for the case of comets. For instance, Kouchi & Kuroda (1990) investigated a mixture consisting of H_2O, CO_2, CO, and CH_4 deposited at 10 K in the ratio 65:10:15:10. All four species are commonly observed in comets (A'Hearn et al. 2012; Dello Russo et al. 2016).The results are reproduced in Fig. 1 and we will refer to this experiment later on.

Another relevant experiment has recently been conducted by Gudipati et al. (2023) and is reproduced in Fig. 2. It included a mixture of H_2, CO_2, CO, and O_2 in the ratio 60:20:10:10. The thickness was estimated to be about 0.25 μm (approximately 1000 monolayers) based on calibrated reference water ice samples. In particular, CO and O_2 seem to be much better trapped in H_2O as opposed to CO_2, that is, they mostly outgass from their CO- and O_2-dominated ice phases below 70 K and then again above 140 K. Only a small fraction is associated with CO_2. Whether or not these ratios change as a function of ice thickness remains to be investigated. The portion of the outgassing occurring from the O_2-dominated ice, however, depends on the initial trapping temperature. In their experiment 10 K was used. Furthermore, also residual species from the vacuum chamber background were tracked. This included N, a fragment of N_2 through dissociative electron impact ionization. As

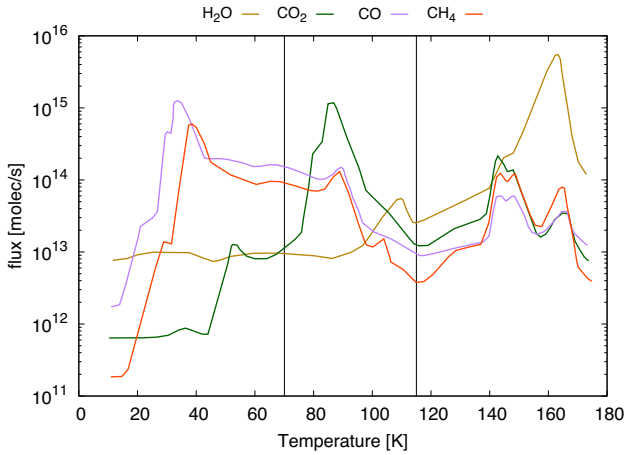

Figure 1. TPD measurement of H_2O, CO_2, CO, and CH_4 after deposition at 10 K in the ratio 65:10:15:10, respectively. Data obtained from Kouchi & Yamamoto (1995). The two vertical lines separate the three temperature regimes introduced in Table 1. The portions released in the three temperature ranges are listed in Table 2.

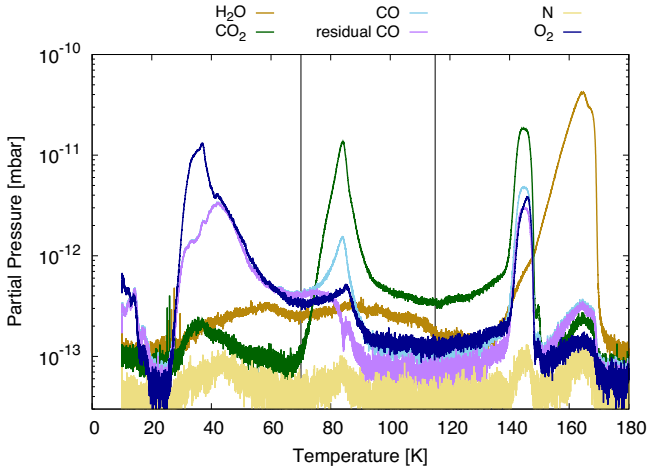

Figure 2. TPD measurement of H_2O, CO_2, CO, and O_2 in the ratio 60:20:10:10, respectively, with a heating rate of 0.5 K min^{-1} (Gudipati et al. 2023). For CO also the residual signal has been derived, that is, after subtraction of the contribution by fragmentation of CO_2. The experiment also tracked the chamber background species N, a fragment of N_2. The two vertical lines separate the three temperature regimes introduced in Table 1. The portions released in the three temperature ranges are listed in Table 3.

in the experiments by Kouchi & Yamamoto (1995), a cryostat set to 10 K was used and also the relative amounts of H_2O, CO_2, and CO were similar.

Additional molecules that have been studied in mixtures of H_2O and CO_2, are NH_3 and CH_3OH (Martín-Doménech et al. 2014). At comet 67P, both molecules can be considered trace species in the ices of the outgassing layer with abundances below the per cent level with respect to H_2O (Rubin et al. 2019b; Läuter et al. 2020).

Kouchi & Sirono (2001) have shown that impurities >2 per cent in the H_2O ices will turn the exothermic behaviour of the amorphous to crystalline ice transitions endothermic, unlike the situation for pure water ice (see e.g. Gudipati et al. 2023). Therefore, a runaway phase transition of amorphous to crystalline water ice cannot be expected for an ice composition characteristic for comets and is hence not a major driver of the outgassing activity.

Table 1. Outgassing behaviour of the H_2O, CO_2, CO, and CH_4 mixture (ratio 65:10:15:10) and the H_2O, CO_2, CO, and O_2 mixture (ratio 6:2:1:1 with residual N_2) according to the TPD measurements shown in Figs 1 and 2 and split into three temperature ranges, separated by the species governing the outgassing: highly volatiles, CO_2, or H_2O.

Temperature range	Released volatile species
< 70 K	Ices dominated by highly volatile species, CH_4, N_2, CO, and O_2, are being released. Marginal co-release of the the lesser volatile molecules CO_2 and H_2O.
70–115 K	CO_2 outgassing with co-desorption of the trapped CO, N_2, CH_4, and small amounts of O_2. Marginal co-release of the lesser volatile H_2O.
> 115 K	CH_4, CO, O_2, N_2, and CO_2 are being released during the amorphous to crystalline H_2O ice transition, that is, the molecular volcano at about 145 K, with a minor contribution of H_2O. The bulk sublimation of H_2O then occurs a few degrees above that with additional release of small amounts of highly volatile molecules.

Table 2. Normalized fractions of release of H_2O, CO_2, CO, and CH_4 in the indicated temperature ranges during the TPD experiment by Kouchi & Yamamoto (1995) shown in Fig. 1.

Temperature range	H_2O	CO_2	CO	CH_4
< 70 K	0.012	0.017	0.756	0.612
70–115 K	0.018	0.782	0.172	0.203
> 115 K	0.970	0.201	0.071	0.185

Table 3. Normalized fractions of release of H_2O, CO_2, CO, N_2 (based on fragment N), and O_2 in the indicated temperature ranges during the TPD experiment from Gudipati et al. (2023) shown in Fig. 2 and after offset-subtraction. For CO the residual signal has been used, that is, after subtraction of the contribution by fragmentation of CO_2.

Temperature range	H_2O	CO_2	CO	N_2 (N)	O_2
< 70 K	0.017	0.015	0.700	0.388	0.816
70–115 K	0.020	0.435	0.071	0.191	0.056
> 115 K	0.963	0.550	0.230	0.421	0.128

Based on the experiments by Kouchi & Kuroda (1990) and Gudipati et al. (2023), which are also qualitatively in agreement with Martín-Doménech et al. (2014), we define the three temperature ranges listed in Table 1 (cf. Figs 1 and 2). The selection of temperature limits is somewhat arbitrary, but for now we will stick to this simplistic approach as it allows for the qualitative comparison of the different data sets. For the following discussion, however, it is important to note that the numbers may change slightly in case different limits are selected. The general behaviour, however, remains the same.

Table 2 lists what fraction of the volatiles shown in Fig. 1 is released in each temperature interval from Table 1. For instance, almost 70 per cent of the CH_4 was in its own phase and then released at or near its pure ice sublimation temperature (cf. Fray & Schmitt 2009), about 14 per cent was released together with CO_2, and the rest was associated with H_2O sublimation, either in the molecular volcano or co-release (Kouchi & Yamamoto 1995). A very similar picture arises for CO. Furthermore, half of the CO_2 was released together with H_2O in these experiments. Similarly, the results from Fig. 2 are collected in Table 3.

Both measurements were obtained using the same deposition temperature and similar relative amounts of host species CO_2 and H_2O. The results generally agree but there are also some differences, for instance, the fraction of the CO_2 co-desorbing with H_2O (in the temperature regime >115 K) is larger in the TPD measurements by Gudipati et al. (2023). On the other hand, the CO fraction released together with CO_2 (i.e. in the temperature regime 70–115 K) is smaller than observed by Kouchi & Yamamoto (1995), especially after subtraction of the fragmentation contribution of CO_2 through dissociative electron impact ionization. Both cases in Figs 1 and 2 show a continuum-type outgassing of CO, O_2, and CH_4 extending from the <70 K regime well into the CO_2-dominated regime. In parts this has to do with the heating rate used for the experiments, which is probably faster compared to the situation at a comet (see later discussion in Section 4). Furthermore, Gudipati et al. (2023) also referred to a limited pumping efficiency of the CO in their vacuum system. In fact, at pressures below 1×10^{-8} mbar during the warm-up phase, it is quite impossible to remove completely the gaseous highly volatile molecules on the time-scale of the experiment. Therefore, surface-bound CO may linger at elevated temperatures after its release, resulting in a higher mass spectrometric signal. This is a commonly known limitation of the TPD technique. Nevertheless, we did not modify our results for such an effect, but taking all this into account, the relative fraction of CO, O_2, and CH_4 that is co-released with CO_2 is likely lower than the numbers provided in Tables 2 and 3. These are complications that we have to keep in mind when putting our measurements at 67P in the context of the laboratory experiments.

4 OBSERVATIONS AT COMET 67P

ROSINA detected and monitored numerous volatiles throughout the Rosetta mission. For the first time, changes in the composition or ratios of the outgassing can be studied with high temporal resolution and excellent coverage in time. In the following, the acquired data set is used to study the behaviour of the different volatiles with respect to each other. But first, we will summarize a suite of observations that are relevant for our study.

4.1 Supporting observations

For comets, we only have limited information about the temperature of the outgassing layer. Gulkis et al. (2015) presented millimetre (mm) and submillimetre (smm) brightness temperatures of the Northern and the Southern hemispheres in the range of 60–180 K, measured by MIRO with spatial resolution down to 40 m when 67P was still beyond 3.2 au. During that time, the Northern hemisphere was in summer and, hence, elevated temperatures were measured compared to the south (cf. Section 2.2). The brightness temperature showed strong spatial variations, mostly associated with illumination and self-shadowing due to the comet's complex shape. On a longer time-scale, this is furthermore coupled with a varying dust cover, for instance through transport and redeposition, changing subsolar latitude, and variation in solar irradiation as a function of the changing heliocentric distance along the comet's orbit.

The MIRO mm temperatures are lower than the smm temperatures, hence mark a decrease in temperature with depth from the comet's surface. In comparison, the maximum diurnal surface temperature in the 2014 August–September time frame was on the order of 230 K inferred from VIRTIS measurements in the infrared spectral wavelength range of $4.5 - 5.1$ μm (Tosi et al. 2019). Compared to the MIRO observations, VIRTIS temperatures would be much closer to the surface, that is, a few tens of micrometre versus approximately a centimetre, respectively. In combination, these results are consistent with a very porous, low bulk thermal inertia nucleus which indicates that pristine material may still be present at relatively shallow depth (Groussin et al. 2019). While the temperatures derived by MIRO may not reflect the actual outgassing layers, Gulkis et al. (2015) suggested that the smm and mm radiation is affected by the temperature at the diurnal thermal skin depth, which they estimated to be on the order of 1–2 cm for 67P at 3.84 au. Other components affecting the temperature are the seasonal skin depth (∼1 m) and the isothermal layer underneath.

Closer to perihelion (1.24 au), however, the solar irradiation was substantially higher. Still, there may be regions on the comet that never reached the amorphous to crystalline ice transition temperature of water, or only during a limited time and within a limited heliocentric distance. This may still have resulted in a slow sublimation of the amorphous water ice together with all the trapped species within. An example is comet Hale-Bopp, for which water activity has been observed even beyond 4 au (Biver et al. 2002). On a temporal scale, thermal gradients up to 0.1 K min^{-1} have been reported for 67P when looking at the averaged brightness temperature (Gulkis et al. 2015). Even higher thermal gradients, locally up to 2–9 K min^{-1}, have been observed by VIRTIS on the surface of regions which experience sudden daytime shadowing (Tosi et al. 2019). Such thermal gradients may lead to strong thermal stresses, for instance in 67P's neck area (Hapi; cf. El-Maarry et al. 2015), where also a water frost cycle has been observed (De Sanctis et al. 2015).

The gas measured by ROSINA may originate from all over the nucleus' surface facing Rosetta due to the large FoV (Section 2.1), even if most of it originates from a much more confined location (Kramer et al. 2017; Läuter et al. 2019, 2020; Combi et al. 2020). But even in small areas the illumination conditions, dust cover, etc. can vary substantially, which greatly broadens up the parameter space for relevant laboratory ice experiments. It is therefore clear that there is no single TPD experiment covering the whole range of conditions encountered at any given point in time. Complications arise from, for example, the distribution of the gas sources across the comet's complex shape coupled with its rotation and orientation of the rotation axis, the variation in heliocentric distance, dust coverage, and thermal gradients in its interior. Hence, it is unlikely that ROSINA measurements can distinguish outgassing caused by the molecular volcano or co-release during the water ice sublimation due to the rather close temperature and close source regions on the comet. Accordingly, ROSINA data do not reveal the exact structure and stratification of the ices. Therefore, when talking about trapping, we not only include ices with incorporated impurities, but also layered ices, where the upper layer quenches the outward diffusion of more volatile species from below. This is based on the thick and thin ice experiments performed by Notesco & Bar-Nun (2005) and discussed above.

Still, a number of conclusions can be drawn for a comet like 67P. In the following, and according to Table 1, we simply consider the 70–115 K temperature regime to be CO_2-dominated and driven. The >115 K temperature regime is assumed to be H_2O-outgassing driven, including both the molecular volcano desorption and co-desorption (Section 3). We assume that the major species, CO_2 and H_2O govern the outgassing behaviour, but will also look for signs, or the absence thereof, of separate ice phases dominated by highly volatile species.

With regards to the observations at 67P, the species provided in Tables 2 and 3 are all relevant. First, they contain the two primary cometary coma molecules, H_2O and CO_2. Then CO, CH_4, N_2 (monitored through fragment N), and O_2. The corresponding pure ice sublimation temperatures are listed in Table 4. There are many more species observed in comets, however, if their sublimation

Table 4. Relative abundances in 67P of H_2O, CO_2, a suite of species with volatility between H_2 and CO_2 (CH_3OH, HCN, and NH_3), and highly volatile molecules (C_2H_6, C_3H_8, CH_4, O_2, and CO), sorted by their pure ice sublimation temperature from Fray & Schmitt (2009) and Behmard et al. (2019) for C_3H_8 (second column). The bulk abundances are given in the third column. Columns four and five show the partitioning in the two main ice phases, H_2O and CO_2. The last column lists the maximum amounts co-released with H_2O (cf. Figs 3 and 7), for exmple, up to 2 per cent of the total 7.5 per cent of the CO_2 can be trapped in or underneath water which corresponds to 27 per cent of the total CO_2.

Species	Sublimation temperature (K)	Bulk abundance (per cent)	Portion with H_2O (per cent)	Portion with CO_2 (per cent)	Max portion with H_2O (per cent)
H_2O	144	100	100	0	–
CH_3OH	142	0.54[a]	–	–	37
HCN	126	0.18[a]	–	–	49
NH_3	102	0.41[a]	–	–	50
CO_2	86	7.5[a]	13	87	27
C_3H_8	83	0.018[b]	6	94	60
H_2S	80	1.8[a]	47	53	48
C_2H_6	68	0.85[a]	5	95	18
CH_4	36	0.43[a]	54	46	70
O_2	30	2.3[a]	99.7	0.3	100
CO	28	3.1[a]	70	30	72
N_2	26	0.089[b]	63	37	79

Notes. The bulk abundances are taken from the mission integrated outgassing [a]from Läuter et al. (2020) where available or from the relative outgassing period just before perihelion [b]from Rubin et al. (2019b).

temperature is higher than CO_2, and possibly even H_2O, they may not be efficiently co-released. For instance, Fig. 1 shows that CO is released with H_2O but not very much the other way round. This, of course, is emphasized due to higher H_2O abundance in the experiment. The same applies to other combinations, for example, both CO and CH_4 are released together with CO_2 but, in relative numbers, only little of the total CO_2 comes off together with CO or CH_4, respectively. Another example is CH_3OH which does no co-desorb with CO (Ligterink et al. 2018). And then there are also numerous species of even lower volatility than water, sometimes even associated with dust (Altwegg et al. 2017b; Hänni et al. 2022).

4.2 H_2O and CO_2

The focus of this section is on the two main ice phases in 67P, H_2O and CO_2. The top left panel in Fig. 3 shows the densities of the two molecules measured by ROSINA at the location of Rosetta versus each other after multiplication by the squared distance to the comet, $r_{\rm dist}^2$, in the following called modified density. This modification has been applied to remove, to first order, the variation in cometocentric distance. The data start 2014 mid-August, just after arrival at the comet and then extends to 2016 September 5, when a dust impact into the DFMS instrument hampered subsequent measurements by physically blocking the current of ionizing electrons (Altwegg et al. 2017b). As a result the data shown here cover a range of heliocentric distances, that is,. from 3.6 au pre-perihelion to 3.7 au post-perihelion. Otherwise, no limitation was applied regarding the position of the spacecraft with respect to the comet and hence the presented data cover a wide range of subspacecraft latitudes and longitudes as well as phase angles.

The top right panel of Fig. 3 shows a time-series of the H_2O and CO_2 densities measured by ROSINA during a period of several weeks late in the Rosetta mission. Both species show a very distinct behaviour, especially between 2016 early and mid-June, a time when Rosetta moved from the terminator orbit (phase angle 90°) to a lower phase angle of about 44° and then back again. Peaks in the measured densities occurred when Rosetta was passing above the continuously more active Southern hemisphere past the outbound equinox (subsolar latitude >5° north). Hence, CO_2 showed a stronger dependence on the subspacecraft latitude than H_2O. As a consequence, this period, which reveals a strong dichotomy between CO_2 and H_2O, is well suited to visualize the different behaviour of the highly volatile species co-released with the two host species.

Fig. 3 also shows the measured H_2O and CO_2 densities for the entire time period analysed (including the detailed view in the top right panel). For most of the time throughout the Rosetta mission, H_2O was the dominant species and H_2O-outgassing followed more or less the subsolar latitude (Combi et al. 2020; Läuter et al. 2020). CO_2, on the other hand, was predominantly released from the Southern hemisphere, in particular also during the early Rosetta mission when the Southern hemisphere was only poorly illuminated (Läuter et al. 2020). The two bottom panels show the corresponding subsolar and subspacecraft latitudes and the heliocentric and cometocentric distances.

As previously reported, for example, by Hässig et al. (2015), Gasc et al. (2017), and Luspay-Kuti et al. (2019) and in line with Fig. 3, both primary cometary parent species, H_2O and CO_2, are only poorly correlated. Part of the remaining correlation shown in the left panel is caused by the strong variation in outgassing activity due to the change in heliocentric distance: both species have their peak outgassing coinciding about 2 weeks after perihelion (points in the upper right corner of the top left panel), whereas farther away (purple: pre-perihelion and yellow: post perihelion) the outgassing of both molecules was significantly lower (Combi et al. 2020; Läuter et al. 2020).

This seasonal evolution is in agreement with observations by VIRTIS, which revealed a change in composition of the comet's surface during the same time frame. Filacchione et al. (2020) and Ciarniello et al. (2022) showed that erosion of the nucleus, caused by enhanced gas and dust activity around perihelion, led to a blueing of the surface resulting from the exposure of more pristine icy layers. Far from the sun, dehydration of the surface combined with the redeposition of dust decreased the amount of ices in the surface layer.

Some degree of the correlation observed in the top left panel of Fig. 3 incurs from just the change in heliocentric distance and hence activity. Nevertheless, water and carbon dioxide abundances show strong variations with respect to each other, in fact the CO_2/H_2O ratio

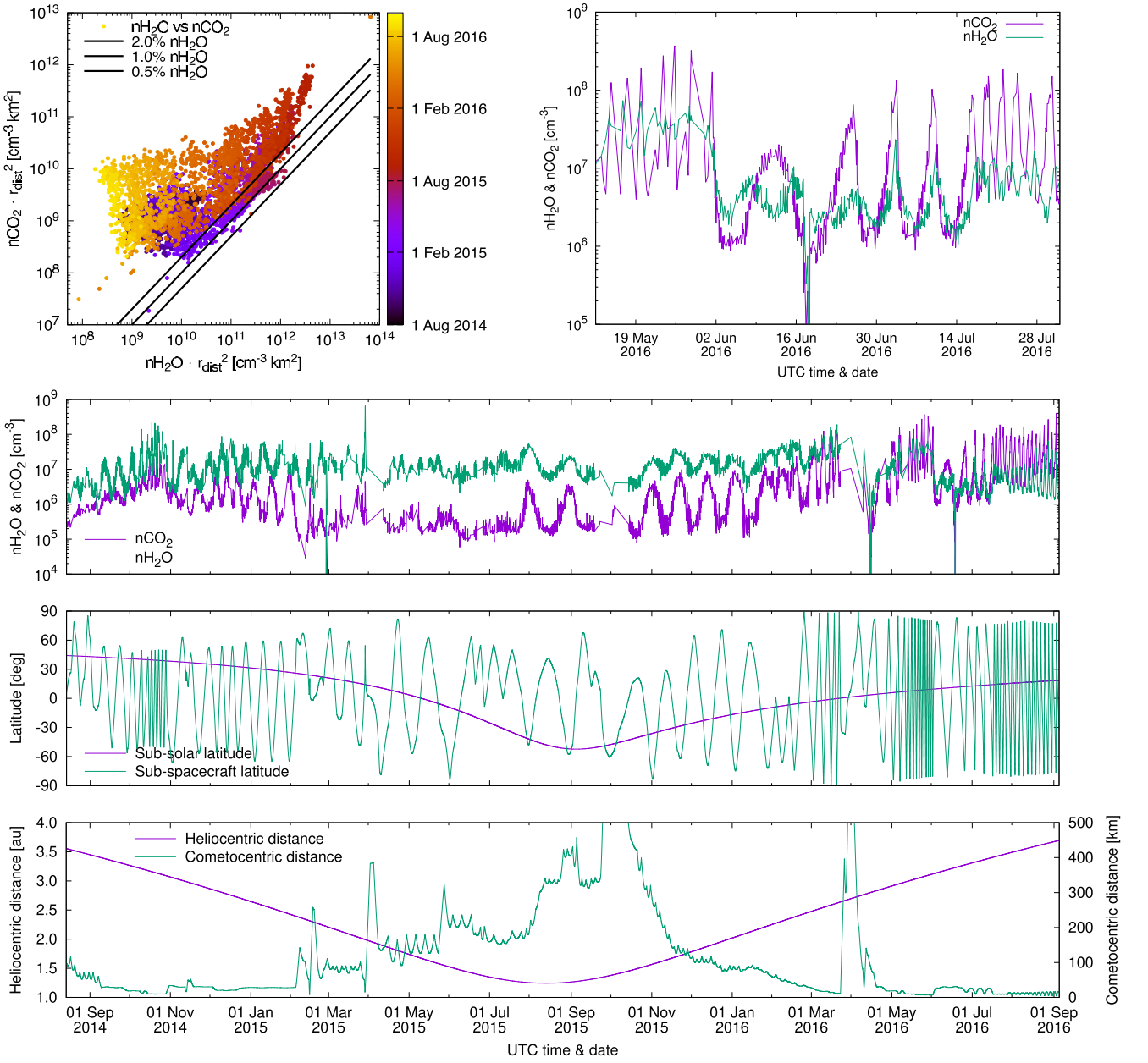

Figure 3. Top left panel: measured H_2O versus CO_2 densities between 2014 mid-August (inbound at 3.6 au), though perihelion (1.24 au), until 2016 September outbound at (3.7 au) and multiplied by the cometocentric distance squared. The dashed and dotted lines mark the minimum CO_2 densities when 0.5 per cent, 1 per cent, or 2 per cent is (trapped in and) co-desorbing with H_2O. Top right panel: H_2O and CO_2 densities measured by ROSINA during close ellipses in summer 2016 when 67P was on its outbound journey near 3.2 au from the sun. For readability, the measurements have been connected by straight lines, despite the measurements being rather sparse during 2016 May/June as different measurement modes were executed, for example, the search for noble gases (Balsiger et al. 2015; Marty et al. 2017; Rubin et al. 2018). The lower three panels, top to bottom: measured H_2O and CO_2 densities during the whole analysed period as shown in the top left panel, the corresponding subsolar and subspacecraft latitudes, and the corresponding heliocentric distance of 67P and the distance between Rosetta and the comet used in the top left panel.

changes by more than two orders of magnitude. While early on in the Rosetta mission, CO_2 could be as low as a few per cent with respect to H_2O, during the final months, when Rosetta was beyond 2.7 au outbound, the carbon dioxide became the dominant molecule in the coma (Läuter et al. 2020). The top right panel, for instance, shows a period where local H_2O and CO_2 abundances were comparable, one dominating over the other at times and then vice versa.

CO_2 has always been present in the coma, even above the deposit layers in the Northern hemisphere, where airfall is expected to be mostly depleted in CO_2 (Davidsson et al. 2021). The top left panel of Fig. 3 also shows lines representing lower limits for the CO_2 when assuming that 0.5 per cent, 1 per cent, or 2 per cent is (trapped in and) co-desorbing with H_2O and reveals no relative abundances of CO_2 with respect to H_2O below 0.5 per cent.

As a consequence, from here on we assume that about 1 per cent of the carbon dioxide is trapped in water. We can compare the 1 per cent CO_2 (w.r.t. H_2O) to the total 7.5 per cent CO_2 from the integrated outgassing over the whole Rosetta mission (Läuter et al. 2020). This

leaves 6.5 per cent CO_2 to be present in its separate (multilayer) phase, that is, in a ratio of 1:6.5, see also Table 4. If, for the sake of comparison, we base our analysis on the bulk abundance of CO_2 of 4.7 per cent (w.r.t. H_2O), derived just before perihelion (Rubin et al. 2019b), the partitioning of CO_2 in H_2O versus a CO_2-dominated phase would be 1:3.7. TPD measurements show that CO_2 is easily trapped in H_2O. The experiment by Kouchi & Yamamoto (1995) in Table 2 revealed a ratio of about 1:4 and Gudipati et al. (2023) in Table 3 obtained approximately 1:1. These ratios depend on the deposition rate and temperature of the experiments in the laboratory and one should be careful in comparing them at face value.

Furthermore, there are also caveats associated with ROSINA measurements: H_2O and CO_2 were measured with a time difference of about 15 min and interpolated in time. Additionally, there are errors related to the measured ratios of ~ 20 per cent originating from sensitivity calibration of DFMS. Therefore, an even higher fraction of the carbon dioxide trapped in water cannot be excluded either.

In the next section, we will study the highly volatile molecules which are co-released with both the H_2O- and the CO_2-dominated ice phases.

4.3 Highly volatile molecules

Here, we discuss the highly volatile molecules CO, CH_4, O_2, N_2, H_2S, C_2H_6, and C_3H_8 that were all commonly observed in the coma of 67P. For this analysis, we limited the data set to the time interval when the Southern hemisphere of the comet was more active than the Northern hemisphere, that is, starting from 2015 early-February inside 2.4 au inbound (Läuter et al. 2020). Only early on in the Rosetta mission, the Northern hemisphere was the dominant source of volatiles in the coma. The Southern hemisphere, on the other hand, showed the highest levels of activity and, hence, erosion due to the short but intense summer around perihelion (Keller et al. 2015). As a consequence, the analysed data mostly represent outgassing from fresh cometary ices that continuously became accessible. As a result, the data shown here cover a range of heliocentric distances, that is, from 2.4 au pre-perihelion to 3.7 au post-perihelion on 2016 September 5. Later on in the Section 4.5, we will then also discuss the omitted early period from 2014 August to 2015 February.

Fig. 4 shows CH_4 in comparison to H_2O and CO_2. The top left panel presents the abundance of CH_4 with respect to carbon dioxide after multiplication with the cometocentric distance squared to account for the variation on cometocentric distance. The second panel shows the same, but relative to water. These modified densities span over several orders of magnitude, therefore the correlation coefficients, listed in the *x*-axis labels, have been fitted after taking the logarithm of the corresponding values to assign equal weights across the decades. The corresponding results were $n\mathrm{CH_4} = 0.064{\cdot}n\mathrm{CO_2}$ and $0.0081{\cdot}n\mathrm{H_2O}$. A perfect correlation would align the points on the diagonal solid black line. The 1-standard deviation bounds (dashed lines) are offset from the diagonal by the indicated factor.

The coefficients can also be compared to the corresponding bulk abundances from Table 4: $n\mathrm{CH_4} = 0.0043{\cdot}n\mathrm{H_2O}$, or when taking $\mathrm{CO_2/H_2O} = 0.075$ into account, follows $n\mathrm{CH_4} = 0.057{\cdot}n\mathrm{CO_2}$. The bulk abundance values (from Table 4 and listed below the *x*-axis labels in the top row of Fig. 4), however, are dominated by the measurements during the most active phase of the mission, independent whether the integrated outgassing over the whole mission was considered (Läuter et al. 2020) or a suitable period pre-perihelion was investigated (Rubin et al. 2019b). As a result, the points reflecting the bulk abundances (2015 August, near-perihelion period in the upper right corner of each panel) are located below the diagonal line in the case of CO_2 (left panel) and H_2O (middle panel). The third panel in the top row shows methane versus a linear combination of water and carbon dioxide, taking into account that 1 per cent CO_2 is associated with H_2O. First, it can be seen that a linear combination of the H_2O and CO_2 densities rather well reproduces the measured CH_4 density: the data points are well aligned diagonally and the corresponding standard deviation is smallest for the right panel, that is, the linear combination reproduces the majority of the measurements within 45 per cent accuracy (within a factor of 1.45 from the diagonal line).

The result of this fitting process is also observed in the bottom two panels: on the left, the reconstructed $[n_{\mathrm{CH_4}} = 0.0023{\cdot}n_{\mathrm{H_2O}} + 0.031{\cdot}(n_{\mathrm{CO_2}} - 0.01{\cdot}n_{\mathrm{H_2O}})]$ versus the measured CH_4 density is plotted for the whole period investigated here. No modification by the cometocentric distance squared has been applied. The panel on the bottom right shows a zoom into the 2016 May to July period for comparison to the right panel of Fig. 3. While the match is not perfect, the behaviour is well reproduced despite the strong differences between the two host species CO_2 and H_2O. Also, we have to keep in mind that the whole 19 months period has been taken into account in the fitting process and not just the 3 months shown in the right panel. In our approach, however, we wanted to investigate the different volatiles' behaviour throughout the comet's orbit and we hence refrain from fitting individual time periods.

The obtained correlation coefficients are now used to assign the partitions of CH_4 related to H_2O versus CO_2, respectively, when again taking the bulk value of $\mathrm{CO_2/H_2O}$=0.075 into account: from $0.0023/(0.0023 + 0.031{\cdot}0.065) = 0.54$ follows that methane can be associated in about equal portions to water and carbon dioxide. For comparison, if we assume that no CO_2 is trapped in or underneath water, follows $0.0023/(0.0023 + 0.031{\cdot}0.075) = 0.50$, which yields a very similar conclusion as indicated already in Section 4.2. The amount of CO_2 that is trapped in or underneath H_2O is hence of secondary importance and does not substantially change our results for the minor species.

A similar picture is obtained for CO in Fig. 5. Also here, the modified CO density can be expressed rather well by a linear combination of the modified H_2O and CO_2 densities. The results reveal a somewhat larger portion of the carbon monoxide, of about 70 per cent, being associated with water compared to 30 per cent with carbon dioxide, respectively.

Another molecule we investigated is molecular oxygen, which is of particular interest as it represents one of the most surprising findings in comet 67P (Bieler et al. 2015; Fulle et al. 2016). O_2 shows a strong correlation with H_2O, which is also reproduced in Fig. B1. Only very little difference is seen between the middle and right panels. Nevertheless, Luspay-Kuti et al. (2022) showed that a small fraction of the O_2 is not correlated to H_2O. This is also reproduced in our analysis, that is, the small portion associated with carbon dioxide can only be observed late in the Rosetta mission, when CO_2 was the dominant species in the coma (cf. Fig. 3).

Our results for N_2, another highly volatile molecule, are provided in Fig. B2 and Table 4. It should be noted that mass-spectrometric interferences, that is, the close mass of CO ($27.9944\,u\,e^{-1}$) to the much lower abundant N_2 ($28.0056\,u\,e^{-1}$), complicates the analysis of the data and increases the uncertainty due to an additionally required peak fitting procedure (see Appendix A). Hence, our results for N_2 include more scatter and fitting errors than the other species investigated in this work. This is, in parts, also reflected in the larger standard deviation we derived. Still, N_2 bears some resemblance to CO, with the larger part associated with H_2O and a smaller fraction with CO_2.

Ethane, presented in Fig. B3 (see also Luspay-Kuti et al. 2019), and propane, presented in Fig. B4, are both well correlated to CO_2,

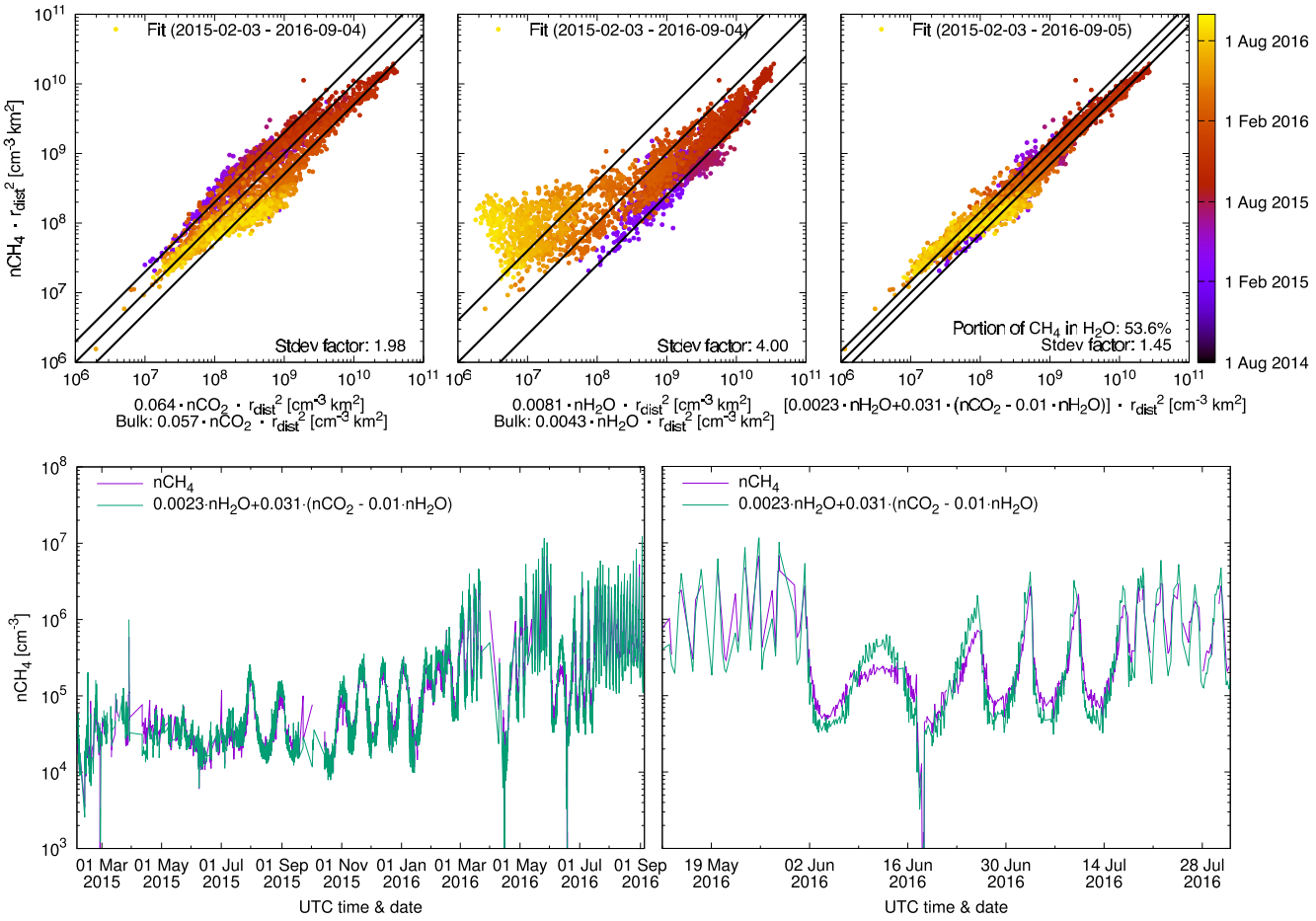

Figure 4. Top row: modified densities of CH_4 versus CO_2 (left), H_2O (middle), and a linear combination of both H_2O and CO_2 (right). Modified density implies multiplication by the cometocentric distance r_{dist} squared to remove, to first order, the distance dependence of Rosetta from the comet. The 1 per cent portion of the CO_2 associated with H_2O has been taken into account in the right panel. The corresponding coefficients were obtained by fitting the log of the data to assign equal weights to the modified densities which cover several orders of magnitude. The results (e.g. $n_{CH_4} = 0.0081 \cdot n_{H_2O}$) can be compared to the reported bulk abundances (e.g. $n_{CH_4} = 0.0043 \cdot n_{H_2O}$, see the text). The 1-standard deviation bounds are provided by the dashed lines (obtained by multiplying and dividing the diagonal solid black line by the indicated factor, respectively). Based on the fitted coefficients from the top right panel it is possible to estimate the portion of the CH_4 that is co-desorbed with H_2O (54 per cent, listed in the panel) versus CO_2 (see also the main text). Bottom row, left panel: CH_4 density measured versus the linear combination from the top right panel, that is, $n_{CH_4} = 0.0023 \cdot n_{H_2O} + 0.031 \cdot (n_{CO_2} - 0.01 \cdot n_{H_2O})$ for the 2015 early-February though perihelion to 2016 September time period. Right panel: zoom-in to the close ellipses in summer 2016 for comparison to the right panel in Fig. 3.

even though some degree of dichotomy is observed for the time period analysed, that is, the early mission values (purple) trend below the diagonal line and later values (yellow) above. This may be a temperature-related fractionation effect, given that the sublimation temperatures of ethane and propane approach the temperature of CO_2, cf. Table 4. Finally, the same analysis has also been carried out for hydrogen sulfide, H_2S in Fig. B5, another species with sublimation temperature close to that of CO_2.

As suggested for the case of ethane, propane, and hydrogen sulfide, the picture for the species of lower volatility changes, that is, when the species' sublimation temperature rises above the one for carbon dioxide. This shall be discussed in the following section.

4.4 Species with volatility between CO_2 and H_2O

As shown in Section 3, species of low volatility seldomly co-desorb with species of higher volatility, for instance H_2O in CO (cf. Tables 2 and 3). Consequently, species like CH_3OH are unlikely to co-desorb in abundant amounts in CO_2 given the substantially higher pure ice sublimation temperature, that is, 142 K versus 86 K, respectively (Fray & Schmitt 2009). On the other hand, CH_3OH does co-desorb with H_2O (Martín-Doménech et al. 2014).

Fig. 6 shows the case of methanol. The top left panel suggests a better correlation of CH_3OH with CO_2 than H_2O (middle panel). The linear combination reveals that about 40 per cent of the methanol would be associated with water. The standard deviation is larger compared to the highly volatile molecules (cf. Section 4.3). Furthermore, the bottom right panel shows that methanol follows much closer the water (cf. Fig. 3) during the low phase angle excursion in the first half of June in 2016. This is in contradiction to the reconstructed density from the coefficients obtained from the linear combination of water and carbon dioxide from the top right panel. Additionally, the bottom right panel also reveals systematically overestimated reconstructed densities compared to the measured methanol densities during the 2016 April to June time frame. In addition, the top right panel also reveals some degree of pre-/post-perihelion dichotomy, although less pronounced than for ethane (Fig. B3). In accordance with the discussion above, methanol rather may be present in its separate ice phase, or correlated with dust grains that contain volatiles, on top of the portion that is trapped in the lesser volatile water.

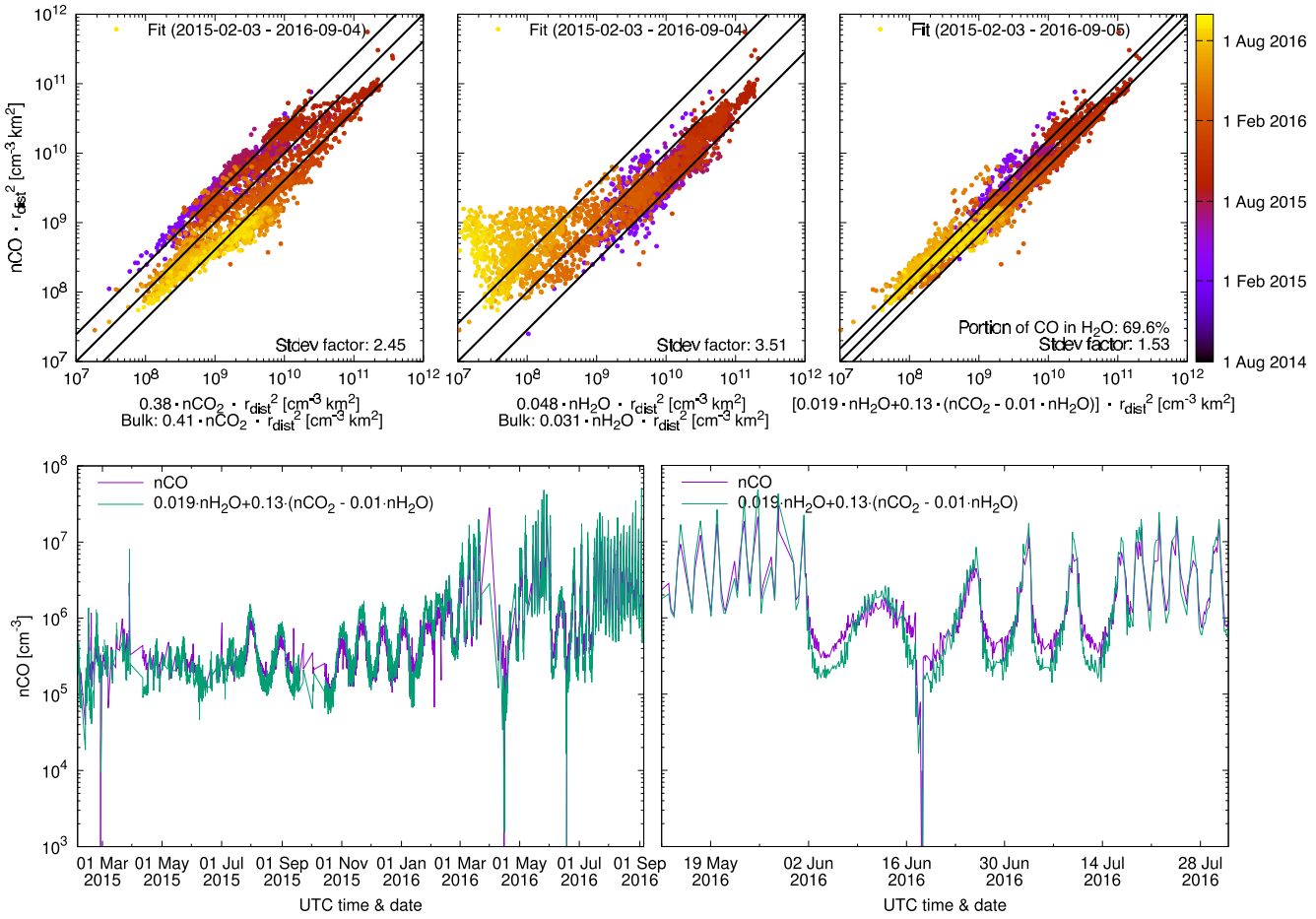

Figure 5. Same as Fig. 4, but for CO instead of CH_4.

Based on data presented here, it is, however, possible to estimate the maximum amount of methanol that is co-released with water. This is based on similar considerations as applied for the CO_2 trapped in or underneath H_2O and shown in Fig. 3. A collection of relative abundances with respect to water for a set of species covering a wide range of sublimation temperatures is presented in Fig. 7. We have also added exploratory lines marking the maximum amounts co-released with water (dashed lines). For instance, only a small fraction of the C_2H_6 can be trapped in or underneath H_2O, otherwise the measured ethane abundance would have to be larger in the 2015 February time frame. On the other hand, pretty much all O_2 can be co-released with H_2O as expected from Fig. B1. In the case of methanol, less than 40 per cent of the density measured at Rosetta may be associated with H_2O. Collings et al. (2004) showed that CH_3OH has water-like desorption characteristics (see also Burke & Brown 2015) on the influence of CH_3OH in water ice. Other relevant TPD experiments by Martín-Doménech et al. (2014) reveal a complicated picture with shifts in the sublimation temperature as a function of experimental heating rate and CH_3OH concentrations in H_2O. Depending on the latter, their results also show a variation in the portion of the CH_3OH outgassing associated with its own (multilayer) ice phase versus co-release with water, ranging from about 1:1 to almost entirely being associated with water. The situation is hence very complex.

Table 4 lists these upper limits for a set of volatiles spanning a considerable range in sublimation temperature. As stated above, these limits are derived by visual inspection only and are associated with relative errors estimated to be on the order of 30 per cent. However, given the complexity of the cometary activity, these limits can still inform us about the incorporated ices and their outgassing behaviour. Consistent with the derived portion associated with the release of water, the upper limits in Table 4 are higher. Just to provide an example, the portion of C_2H_6 stored in H_2O is small, that is, 5 per cent of the total (hence 95 per cent is associated with CO_2), but still smaller than the upper limit of 18 per cent derived from Fig. 7.

4.5 Early mission

In the previous sections, we limited the data to the 2015 February to 2016 September time period when outgassing from the more pristine Southern hemisphere dominated. In this section, we start 2014 mid-August, the time of arrival of the Rosetta spacecraft at comet 67P. Fig. 8 shows the measured (purple) and the reconstructed densities (green) of the highly volatile molecules CO, CH_4, C_2H_6, C_3H_8, O_2, and H_2S.

The reconstructed densities use the fitted parameters obtained in the previous Section 4.3 (cf. Table 4) and were applied to the full time interval. The first key observation, with regard to the early mission phase from 2014 mid-August to 2015 early-February, is that the amount of CO is underestimated. O_2, which shows a strong correlation with H_2O, remains well reproduced. CH_4, C_2H_6, C_3H_8, and H_2S, which exhibit higher degrees of correlation to CO_2, are all overestimated in their reconstructed density. Hence, for the early

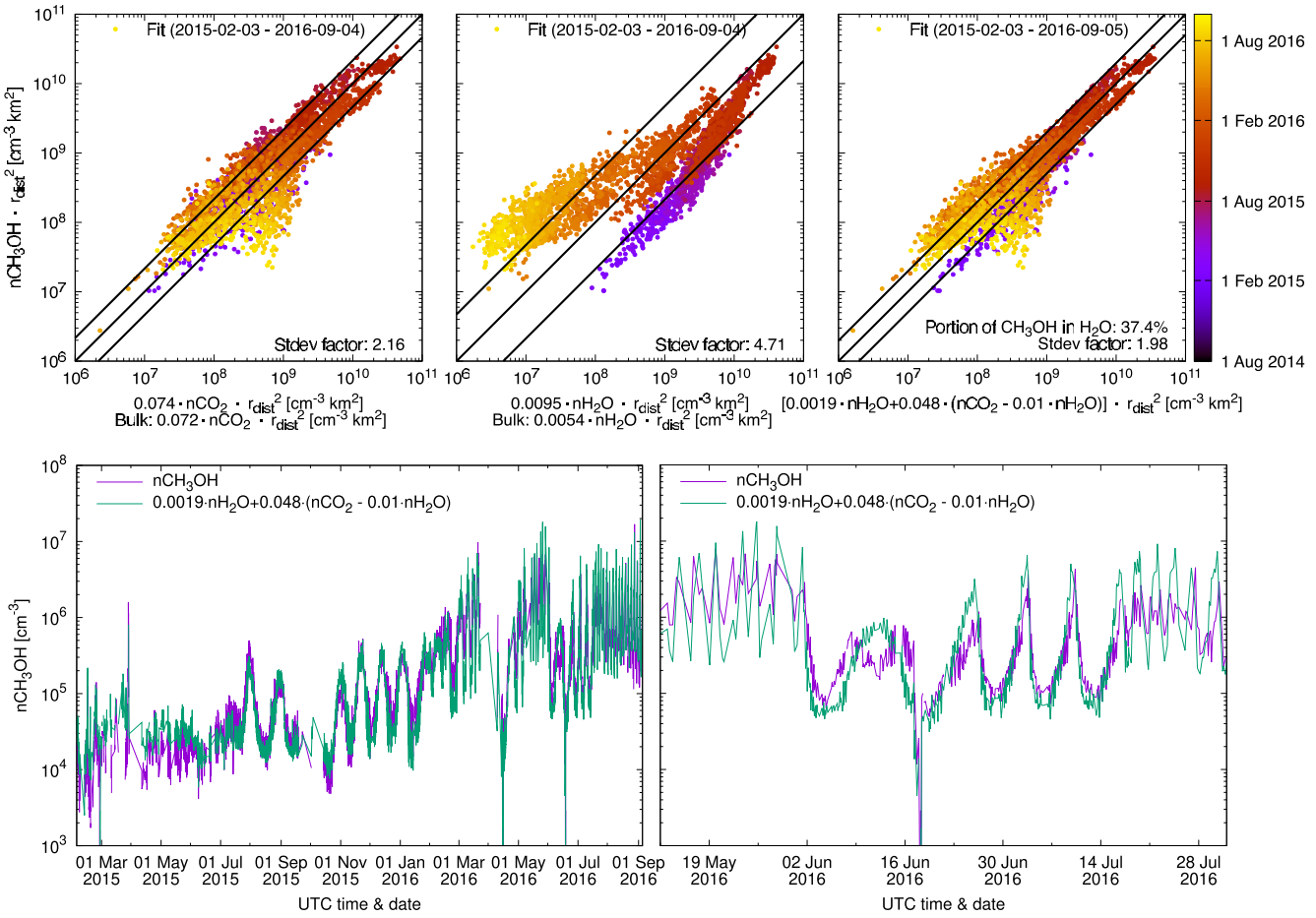

Figure 6. Same as Fig. 4, but for CH_3OH instead of CH_4.

mission phase, we have divided the coefficient reflecting the co-release of the highly volatile molecules in CO_2 by a factor 7 and added the corresponding early-mission reconstruction (blue). This correction factor is just an approximation and not an individual fit for each of these highly volatile molecules. Still, the key point here is that the resulting modified reconstruction shows that the early inbound phase is very distinct from the rest of mission, that is, the CO_2 measured early was most likely depleted in trapped highly volatile species. The coefficient representing the co-release with H_2O, on the other hand, was left untouched. The implications of these observations are discussed in the next section.

5 DISCUSSION

This section combines the findings of TPD reference measurements from the literature and our gas coma observations with the goal to study the outgassing behaviour of a comet like 67P and to improve our understanding of the ices inside its nucleus. Furthermore, we are interested in the potential differences between families of comets resulting from their distinct dynamical history.

5.1 Measurement limitations

Before the discussion of the data presented in the previous section and the comparison to relevant laboratory measurements, there are some limitations to be mentioned. For instance, the relative abundances of the different volatiles used for the TPD measurements do not exactly match the situation of 67P. As mentioned earlier, we investigated the local gas densities at Rosetta and do not directly probe the ices inside the nucleus. We did not include any corrections to the measured gas densities due to gas velocities varying with heliocentric distance, among species, and sources on the nucleus of 67P. Close to perihelion, when the near-nucleus gas densities are highest, the different gas species may be collisionally coupled while this effect plays only a minor role when the comet is far from the sun (Tenishev, Combi & Davidsson 2008). Also, our modified gas density assumes a simple $r_{\rm dist}^{-2}$ density dependence on the cometocentric distance which can only serve as an approximation.

5.2 Trapping of volatiles in H_2O and CO_2

First, we are interested in the behaviour of species of high volatility and their relation to the two main species, CO_2 and H_2O. As reported by Gasc et al. (2017) and Luspay-Kuti et al. (2019) and shown in Fig. 7, no clear distinction between polar and apolar molecules can be made for comet 67P. For instance, H_2O (polar) correlates well with O_2 (apolar) and NH_3 (polar) but not with C_2H_6 (apolar) and CH_3OH (polar). Furthermore, no clear separation according to the pure ice sublimation temperature can be observed, for example, CH_4 can be attributed in similar portions to CO_2 and H_2O, whereas C_2H_6 almost entirely co-desorbs with CO_2. Of course, the situation is more complicated as some of these species may also be linked because of

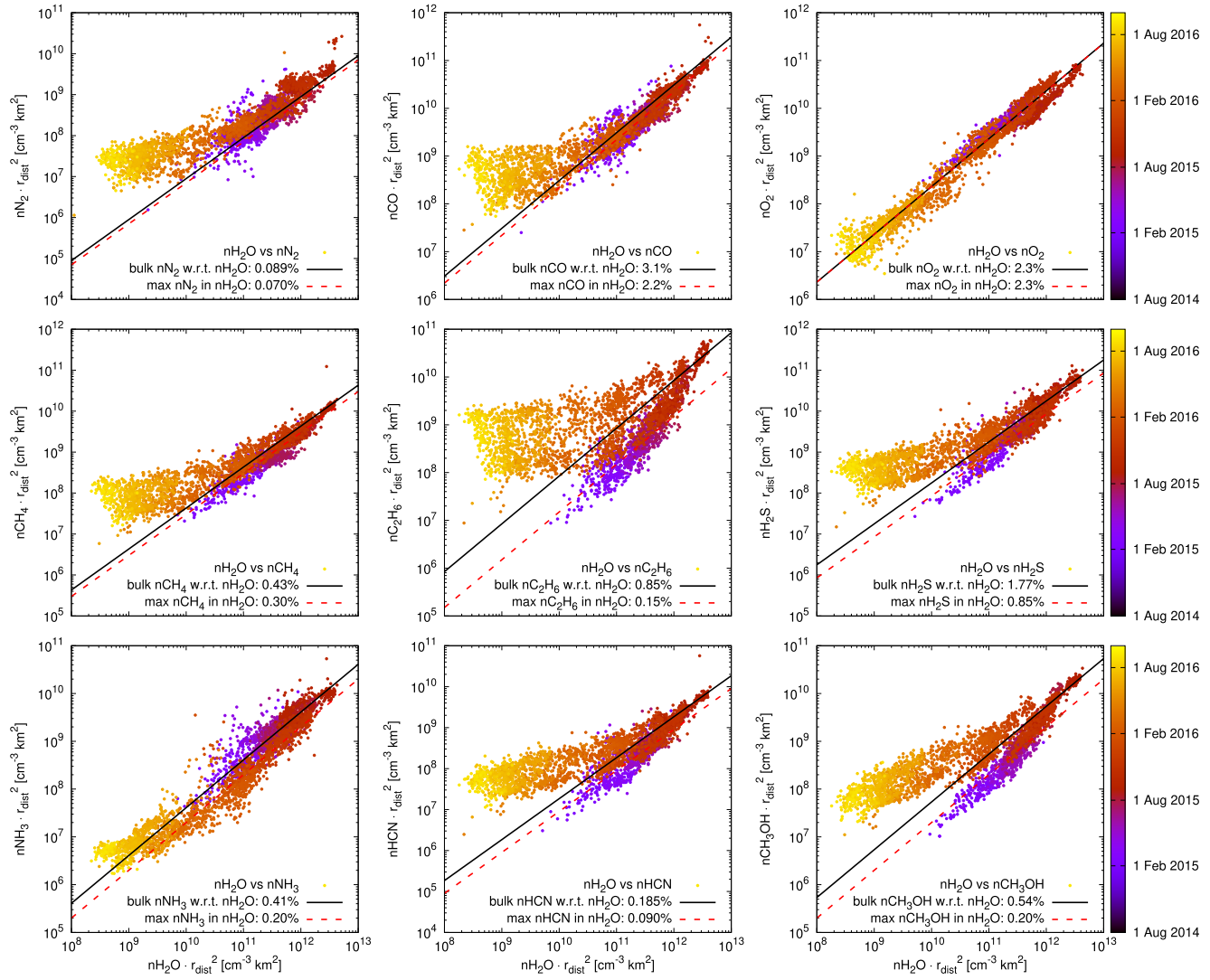

Figure 7. A set of cometary molecule densities plotted versus water between 2015 February and 2016 September after multiplication by the cometocentric distance squared (similar to the left panel of Fig. 3). The solid line refers to the bulk abundance with respect to water which tends to be close to the peak outgassing period around perihelion (points in the top right corner of each panel). The dashed line corresponds to an estimated maximum fraction of a given species that is co-released with H_2O (see the text).

chemical formation while others are not (Herbst & Van Dishoeck 2009).

On the other hand, the local abundance of highly volatile molecules in the coma of 67P, that is, with a pure ice sublimation temperature below CO_2, can be described as a linear combination of the local H_2O and CO_2 densities. Ice phases dominated by highly volatile species cannot be excluded, however, they are not required to explain the measured abundances in the coma. The majority of highly volatile molecules are associated with H_2O and CO_2 in varying proportions. The observed slopes of the different highly volatile molecules reported by Gasc et al. (2017), that is, the heliocentric distance dependence of their outgassing (cf. Section 2.2), can be confirmed to be the result of the slopes of the two main species, H_2O and CO_2, and the corresponding associated fractions.

The *in situ* coma measurements obtained with ROSINA cannot resolve the release of gases in the temperature range of the molecular volcano compared to the main H_2O outgassing peak, which occurs at slightly higher temperatures. As shown in both Figs 1 and 2, when just focusing on the temperature range of the molecular volcano, all trapped volatiles are released together during the amorphous to crystalline ice phase transition. For instance, O_2 would rather be correlated with CO_2 than H_2O. However, we observed only very little of the O_2 to be associated with CO_2 (Table 4). This indicates that the co-release of O_2 and CO_2 during the molecular volcano has only a minor influence on the observed correlations, that is, was accounted for by attributing 13 per cent of the total CO_2 to the co-release with water and subtracting this in our fitting procedure (Section 4.2).

Species of lower volatility than CO_2, on the other hand, may be trapped in or underneath H_2O and be present in their own (multilayer) ice phase. Our analysis yields upper limit estimates for the fraction co-released with water and the results are consistent with the coefficients associated with co-release with water from the linear fits (Table 4). There may also be a transition regime for species with sublimation temperature close to CO_2 as they may co-release with both water and carbon dioxide as well as forming their own phase. Possible candidates are C_2H_6 (cf. Fig. B3), C_3H_8 (cf. Fig. B4), and

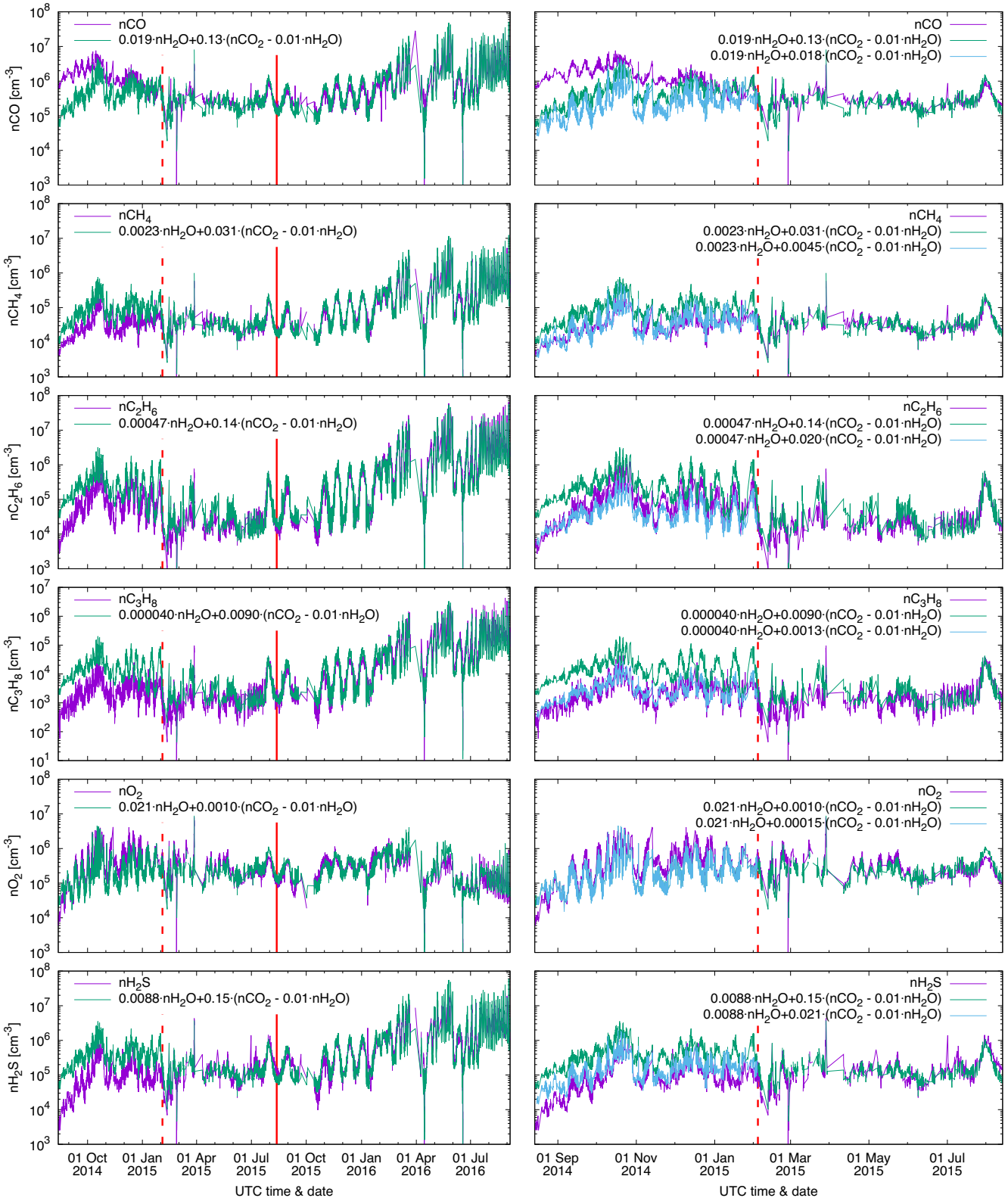

Figure 8. Gas densities of highly volatile molecules measured at the Rosetta spacecraft. The left column shows the measured (purple) and reconstructed densities (green) for the entire analysed period. Perihelion is marked with a vertical solid line. The right column shows the same up to perihelion and adds a curve representing reduced trapping in CO_2 (blue, see also legend and main text) for the time period when the Northern hemisphere was more active (up to 2015 early-February, cf. Läuter et al. 2020, dashed line). Top to bottom: CO (cf. Fig. 5), CH_4 (cf. Fig. 4), C_2H_6 (cf. Fig. B3), C_3H_8 (cf. Fig. B4), O_2 (cf. Fig. B1), and H_2S (cf. Fig. B5).

Table 5. Lost fraction (per cent) of highly volatile molecules, if originally trapped at 10 K and subsequently heated to 70 K, for example, for 67P during the Centaur phase (∼ 7 Myr at 7 au; Guilbert-Lepoutre et al. 2016). CH_4 was taken from Table 2 and O_2, N_2, and CO from Table 3.

Species	Lost fraction (per cent)
CH_4	61
O_2	82
CO	70
N_2	39

H_2S (cf. Fig. B5) which show some degree of pre- to post-perihelion difference (cf. Section 4.3).

5.3 Loss of highly volatile species through thermal processing

In the previous section, we showed that the measured abundances of highly volatile molecules can be explained by trapping in or underneath both water and carbon dioxide. The presented fits do not include an additional component representing the ice phase dominated by the highly volatile molecules CH_4, CO, etc. The first row in both Tables 2 and 3 lists the fraction of the volatiles released in the temperature range <70 K. According to these results, O_2, CO, and CH_4 are all heavily affected and to a lesser extent also N_2. Substantial amounts of these species would hence have been lost from the cometary nucleus of a JFC like 67P prior to arrival in the inner solar system. For the presented TPD measurements, with a trapping temperature of 10 K, the results are summarized in Table 5. With subsequent heating to ∼70 K after trapping, a comet like 67P would have lost up to 70 per cent of its initial CO content.

Nevertheless, our knowledge of the initial trapping temperature or range thereof is very limited. The lost fraction of highly volatile species very much depends on the conditions during trapping. Additional constraints on the temperature during the formation of the material incorporated into 67P may thus be required. These can be obtained from independent considerations: for instance, a chemical reaction model for dark clouds by Taquet et al. (2016) suggests that temperatures of approximately 20 K, which is somewhat elevated compared to typical dark cloud temperatures (5–10 K), may be required to enhance the O_2 abundance to be comparable to the one found in 67P (Bieler et al. 2015). In summary, it remains unclear how much of the highly volatile species were initially trapped and subsequently lost during the dynamical history of the comet.

Thermal modelling, for example, by De Sanctis, Capria & Coradini (2001) and Parhi & Prialnik (2023), shows that substantial amounts of CO-dominated ices will be lost from cometary nuclei in the Kuiper belt at distances beyond 40 au. Loss of the ice phase of highly volatile species may already occur earlier, for instance due to collisional heating during the formation of the Kuiper belt (Jutzi & Michel 2020). Thermal processing of icy primordial disc objects also took place before scattering to the different cometary reservoirs occurred as a result of giant planet migration (Gomes et al. 2005). For instance, Davidsson (2021) found that objects in the size range of 4–200 km would lose their CO-dominated ice content within 0.1–10 Myr due to heating by the protosun and long-lived radionuclides. For small objects, the latter may be less efficient, as shown by Mousis et al. (2017). Furthermore, an early loss of the N_2- and CO-dominated ices is in line with the finding that the N_2/CO ratio is independent of the number of inner solar system crossings (Anderson et al. 2023) given that the outgassing of both highly volatile molecules is governed by the lesser volatile CO_2 and H_2O. For this, we assume that the CO_2/H_2O ratio does not change significantly from one perihelion passage to the next. For the same reason, however, the N_2/CO ratio may change over a single orbit due to the change of the CO_2/H_2O ratio as a function of heliocentric distance. This may then also explain the variation in the N_2/CO ratio observed in 67P (Rubin et al. 2015, 2019b).

The thermal history of a comet similar to 67P may lead to additional depletion of highly volatile species. Here, it is important to consider the dynamic history of 67P (Maquet 2015). Before becoming a JFC, 67P may have spent several million years as a Centaur at an intermediate heliocentric distance around 7 au and undergone internal heating to temperatures of up to 70 K (Guilbert-Lepoutre et al. 2016). This can be compared to comet 29P/Schwassmann-Wachmann 1, a Centaur on its way to become a JFC (Sarid et al. 2019), which shows substantial and routinely detected CO-outgassing (Crovisier et al. 1995). As a consequence, CO may have been another major species in cometary ices, along with H_2O and CO_2, before substantial amounts were lost due to the heating processes. Accordingly, some of the comets originating from the Oort cloud, for example, 1P/Halley (Eberhardt 1999), exhibit higher relative CO abundances compared to CO_2. Also long-period comet (LPC) C/2016 R2 (PanSTARRS), a returning object originating from the Oort cloud, showed both strong N_2^+ and CO^+ emission bands (Opitom et al. 2019). In the ISM, for comparison, CO has been shown to be high in abundance, both in the gas and the ice phases (Boogert, Gerakines & Whittet 2015; Zamirri et al. 2018). As discussed earlier in Section 3 and shown by Parhi & Prialnik (2023), if ample time is available, the same highly volatile species may be also lost at much lower temperatures. We therefore state that the 70 K internal temperature mentioned above is just an upper limit.

These conclusions are compared to those of A'Hearn et al. (2012), who investigated the $CO/CO_2/H_2O$ composition of comets. Their survey includes, aside from JFCs, also LPCs and Halley-type comets (HTCs). The collection of observations shows a large variation in relative abundances of the three species within each of the families of comets, which is hence most likely not the result of their different dynamical origin. Little systematic difference between the families of comets were observed, that is, between JFCs, which reside as a Centaur for an extended period at intermediate distance (Guilbert-Lepoutre et al. 2016), versus LPCs and HTCs. The CO/H_2O ratio did, however, trend to somewhat higher ratios for LPCs when compared to JFCs. However, the two orders of magnitude variation in CO/H_2O in the sample of comets analysed by A'Hearn et al. (2012) complicates the identification of clear trends.

To further delve into this issue, Fig. 9 shows a collection of measured CO abundances with respect to H_2O in both JFCs and OCCs based on infrared spectroscopic (Dello Russo et al. 2016) and *in situ* mass spectrometric observations (Eberhardt 1999; Rubin et al. 2019b). While the ratios are limited to several per cent in JFCs, the variation of CO/H_2O in OCCs is substantially larger. The latter family includes a subset with much higher CO/H_2O ratios. This may be the result of the aforementioned transition through the Centaur stage and other thermal processes related to their dynamical history and possibly the size of the objects, for example, heating due to the collisional cascade in the primordial disc (Davidsson 2023). Consequently, our results support the suggestion by Gasc et al. (2017) and Davidsson (2021) that highly volatile species, such as CO, are trapped in (or underneath) less volatile species like H_2O and CO_2 to remain present in comet 67P's nucleus.

There still remain questions regarding the evolution of comets and associated loss of highly volatile species, for instance, Harrington

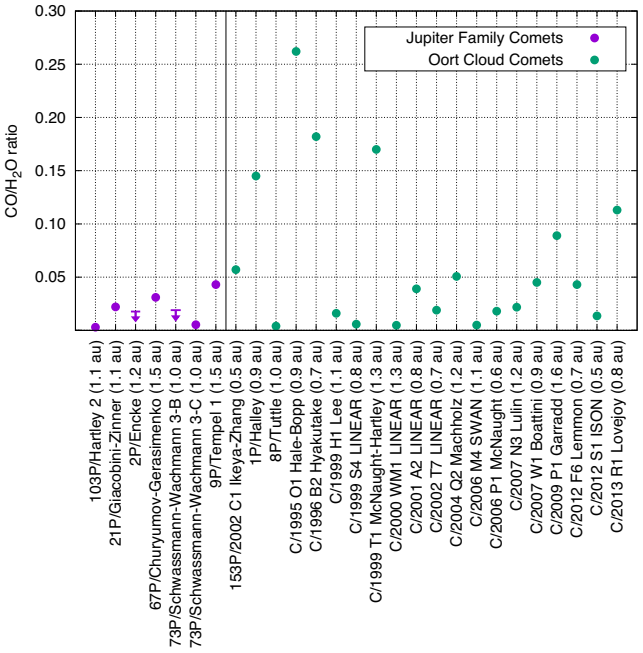

Figure 9. CO/H_2O ratio measured in range of JFCs and OCCs based on infrared spectroscopic observations (Dello Russo et al. 2016), amended by the two comets for which mass spectrometric measurements are available, that is, 1P/Halley and 67P, Eberhardt (1999) and Rubin et al. (2019b), respectively. The label also contains the heliocentric distance of the corresponding observation.

Pinto et al. (2022) reported lower CO/CO_2 ratios in Dynamically New Comets (DNCs) compared to the more processed OCCs. Furthermore, this ratio may even increase with the dynamical age of the comet (A'Hearn et al. 2012). A possible explanation is the irradiation of a DNC by GCRs (Galactic Cosmic Rays) leading to a depletion of the CO in the top layer (Gronoff et al. 2020; Maggiolo et al. 2020) which is then shed during the first apparition.

Luspay-Kuti et al. (2022) reported that the original O_2, regardless of its origin in the ISM or in the PSN, may have been incorporated into the comet at abundances lower than what is found today. They investigated DFMS data obtained during select time periods above 67P's Southern hemisphere at heliocentric distances >2.4 au. In their scenario, evolutionary processing involving secondary trapping in the underlying H_2O matrix leads to the elevated ratio observed by Rosetta. This is somewhat different from the scenario discussed here, which is based on data from almost the entire mission including perihelion and the northern latitudes. Depending on the formation temperature, it is likely that highly volatile species were more abundant in comet 67P after its formation. Also, our scenario to explain the O_2 observations at 67P does not include the formation of a secondary reservoir but the primordial trapping of O_2 in mostly H_2O, with a small fraction in CO_2, similar to the corresponding TPD experiments by Gudipati et al. (2023).

Another key element is nitrogen: cometary volatiles seem to lack a substantial fraction of elemental nitrogen with respect to solar relative abundances of other volatile elements like C and O (Geiss 1988). Several processes have been discussed in the literature, for instance the incorporation of N-bearing species, predominantly NH_3, into ammonium salts of lower volatility (Altwegg et al. 2020). As previously discussed in the literature (e.g. Geiss 1988), the loss of N_2 may also be responsible for a part of the missing nitrogen. Our finding that the measured molecular nitrogen abundance in 67P can be reproduced without including an N_2-dominated phase further supports this scenario. On the other hand, the amount of N_2 lost is limited (Table 5) and not sufficient to explain the nitrogen deficiency alone.

Table 5 also suggests that loss of the ice phase dominated by the highly volatile species is expected to change their ratio as the nucleus undergoes collisional and thermal heating processes. For instance, the N_2/CO ratio may be evolutionary altered which increases the uncertainty when deriving the formation temperature of the incorporated ices (Rubin et al. 2015).

An interesting observation in this regard is the apparently distinct behaviour of the hydrocarbon species investigated in this work. Methane, ethane, and propane have pure ice sublimation temperatures below carbon dioxide (Table 4). Ethane in Fig. B3 and propane in Fig. B4 are well correlated to CO_2, as opposed to H_2O, which is quite distinct from the 1:1 partitioning found for methane according to Fig. 4. This, however, may be explained by the loss of the methane-dominated phase, which may amount to approximately 60 per cent of the total according to Table 5. Therefore, when taking into account the lost portion, the fraction of the total CH_4 which is associated with H_2O would reduce to about 19 per cent (cf. Table 2), which is closer to the partitioning of ethane and propane (∼5–6 per cent associated with H_2O). While we lack reference TPD measurements for ethane and propane in a mixture of CO_2 and H_2O, their pure ice phase sublimation temperature is much closer to the temperature the comet may have witnessed in its past or even close to CO_2 and hence a substantial fraction of the ethane- and propane-dominated ice may still be present inside the nucleus. The preferential loss of methane over ethane is supported by Parhi & Prialnik (2023), who applied a comet evolution model to compute depletion times for different volatiles in Kuiper belt objects (KBOs). Further relevant are the results by Schuhmann et al. (2019), showing that methane and ethane have very similar abundances in the coma of 67P, while other, heavier aliphatic hydrocarbons such as propane showed abundances decreasing with the mass of the molecule. A similar picture was also obtained near perihelion by Hänni et al. (2022). At that time, a substantial amount of cometary dust was present in the coma.

One caveat is that the sublimation temperature of ethane is also close to carbon dioxide (Table 4). This may result in a correlation between the two without causation. In fact, the top right panel in Fig. B3 does reveal some degree of pre-to-post-perihelion difference, similar to H_2S (Fig. B5) and C_3H_8 (Fig. B4), both species with sublimation temperatures even closer to CO_2.

In summary, the presence of highly volatile molecules in comets is, hence, a less stringent limit on the degree of internal heating that could have occurred. Not suitable to recover the thermal history of the comet may be the ortho-to-para ratio (OPR) in water and other molecules: previously, the OPR has been employed to obtain the formation temperature of the ices incorporated into a comet. However, recent work has questioned this connection by showing that the OPR measured in, for example, coma H_2O and NH_2 is independent of the original ice formation process (Shinnaka et al. 2016; Faggi et al. 2018; Cheng et al. 2022).

Other constraints are required, for instance, the limited deuterium-hydrogen isotope exchange reactions, which become significant above temperatures of 70 K on time-scales of 1×10^4 yr (Lamberts et al. 2015). For a comet like 67P, with very different D/H ratios in water when derived from $D/H = 0.5 \cdot HDO/H_2O$ versus $D/H = 2 \cdot D_2O/HDO$ (Altwegg et al. 2017a), this indicates that its internal temperature remained well below 70 K for most of its lifetime.

Another constraint is obtained from the chemical model by Taquet et al. (2016), who suggested a formation temperature on the order of ∼20 K based on the O_2/H_2O ratio measured in 67P (Bieler et al. 2015).

5.4 Comparison with TPD measurements

After neglecting the outgassing in the <70 K temperature range (cf. Table 1), the obtained correlation factors can be compared to the TPD measurements in Tables 2 and 3. We thus estimate the portions of N_2, O_2, CO, and CH_4, respectively, associated with CO_2 (70–115 K temperature range) and H_2O (>115 K temperature range). For instance, based on the TPD measurements by Kouchi & Yamamoto (1995) in Table 2, the portion of the CH_4 outgassing associated with CO_2 is 0.203/(0.203 + 0.185) = 52 per cent which leaves 48 per cent to H_2O. The corresponding result from our fitting procedure of the relative abundances in 67P is 46 per cent of the CH_4 associated with CO_2 and 54 per cent to H_2O (see Fig. 4). For CO, and based on the TPD results by Kouchi & Yamamoto (1995) in Table 2, the portion of the outgassing associated with CO_2 is 0.172/(0.172 + 0.071) = 71 per cent and the remaining 29 per cent are released together with the H_2O. When using TPD measurements from Gudipati et al. (2023) in Table 3, however, 24 per cent are associated with CO_2 and 76 per cent to H_2O. The corresponding results for 67P are 30 per cent of the CO associated with CO_2 and 70 per cent to H_2O (see Fig. 5).

A collection of these results is presented in Table 6. The top two rows summarize our results for 67P, using two different CO_2/H_2O ratios, once from the integrated total relative outgassing during the whole Rosetta mission (Läuter et al. 2020) and once measured pre-perihelion just before the peak outgassing period (Rubin et al. 2019b). The bottom two rows show the corresponding TPD measurements (Kouchi & Yamamoto 1995; Gudipati et al. 2023). It becomes obvious that there is no single TPD measurement that matches the ratios measured for 67P. This, however, is no surprise given that the volatiles measured by ROSINA at 67P originate from various locations which hence cover, among others, a wide variation of local temperatures, ice composition, and depths from which the sublimation occurs (Combi et al. 2020).

5.5 Impact of hemispherical transport of icy grains

Once the Southern hemisphere became active, a fraction of the grains which contain volatiles were entrained in the gas flow, lifted and transported to the Northern hemisphere, and then deposited due to gravity and lower gas drag. The Northern hemisphere is thus subject to redeposition of material and is hence less pristine. Such hemispherical transport of icy grains has been observed and is tied to the prominent deposit regions in the northern regions of the comet (El-Maarry et al. 2015; Thomas et al. 2015; Keller et al. 2017). The Southern hemisphere, on the other hand, is dominated by erosion processes which continuously expose fresh material from the comet's interior (Keller et al. 2015).

Davidsson et al. (2021) showed that H_2O ices are likely to survive this journey, as opposed to the CO_2-dominated phase, which may be lost even from large decimeter-sized chunks of ice. ROSINA measurements show that there are still substantial amounts of CO_2 present in the coma above the north. Our results thus support that at least parts of the CO_2 is trapped in H_2O and hence survives the journey to the Northern hemisphere deposits where it is then released together with the water, consistent with the model by Davidsson et al. (2021).

Another effect that may be contributing to non-zero CO_2 abundances everywhere in the coma are interparticle collisions and surface scattering processes which redistribute molecules around the nucleus, potentially reaching Rosetta even if there is no direct line of sight to the corresponding source region. This effect is expected to be more prominent near perihelion, when coma densities were high and collisions more frequent (cf. Combi et al. 2012). However, the lowest CO_2/H_2O ratios were measured well before perihelion at distances >2 au (cf. Fig. 3), showing that collisions were not the main cause for the minimum abundance of CO_2 which was present throughout the coma.

5.6 Seasonal CO_2 frost

Our fits from Section 5.2 can be applied throughout most of the Rosetta mission, covering a wide range in heliocentric distances, except the early period from 2014 August to 2015 February. As a result of the comet's substantial obliquity of the spin axis (Sierks et al. 2015), 67P exhibits strong seasonal outgassing (Hässig et al. 2015). During the inbound part of the orbit, the subsolar latitude gradually moved from the north towards the south (Fig. 3). Läuter et al. (2020) showed that early in the mission CO_2 sublimated mostly from the south, whereas H_2O followed the subsolar latitude and thus originated during that time from the Northern summer hemisphere. The CO_2, however, appeared to be depleted of highly volatile molecules, possibly due to the sublimation and re-freezing of the CO_2 during the previous outbound arc, when the interior of the nucleus was still warmer compared to the Southern hemisphere surface which gradually went into shadow. However, the embedded highly volatile species released at the same time would not be re-trapped or frozen out efficiently and hence be lost. In fact, the VIRTIS instrument directly observed such patches of CO_2 frost on 67P's surface as they emerged from local winter (Filacchione et al. 2016). The CO_2 frost observed by ROSINA, on the other hand, may not be limited to the surface but also originate from well below. Aside from CO_2, VIRTIS observations by De Sanctis et al. (2015) also revealed H_2O surface frost acting on a diurnal time-scale (cf. Section 4.1).

For the rest of the Rosetta mission, CO_2 remained outgassing predominantly from the south, in particular also after the outbound equinox in 2015 March, despite the subsolar latitude moving back to the northern latitudes (Läuter et al. 2019).

When investigating the absolute production rates, CO_2 showed an almost stable, possibly even slightly decreasing gas production inbound from >3.5 to ∼2.5 au (Combi et al. 2020; Läuter et al. 2020). Again, this may be the result of the CO_2 frost, released from greater depth and re-freezing closer to the colder surface during the previous outbound journey. After aphelion and inbound during the next orbit, the heat wave starts again from the surface inwards and releases the seasonal CO_2 frost, which is now located closer to the surface and devoid of trapped highly volatile species. This, in essence, enhances the comet's early CO_2 activity. Only inside ∼2.5 au, the CO_2 production clearly increased with decreasing heliocentric distance. This then marks again the point when outgassing of fresh and more pristine CO_2, with all of the trapped volatiles, starts.

If we assume that all the CO_2 emitted from the Southern hemisphere before 2015 February, the period for which we found low amounts of highly volatile molecules co-released with CO_2, is frost, then we can estimate the amount of CO_2 frost stored in 67P. For this purpose, we integrate the Southern hemisphere CO_2 production from Läuter et al. (2019) during this early inbound phase and compare

Table 6. Relative portion of highly volatile molecules associated with either H_2O (release in the >115 K temperature range) or CO_2 (70–115 K) from TPD measurements and observed in 67P. For the latter, the results were derived once using the CO_2/H_2O ratio from the mission integrated outgassing (Läuter et al. 2020) and once from the relative outgassing during the period just before perihelion (Rubin et al. 2019b).

	CO_2	CO		CH_4		N_2		O_2	
Associated species (temperature regime)	H_2O (per cent)	H_2O (per cent)	CO_2 (per cent)	H_2O (per cent)	CO_2 (per cent)	H_2O (per cent)	CO_2 (per cent)	H_2O (per cent)	CO_2 (per cent)
67P for $CO_2/H_2O = 0.075$ (Läuter et al. 2020)	13	70	30	54	46	63	37	99.7	0.3
67P for $CO_2/H_2O = 0.047$ (Rubin et al. 2019b)	21	80	20	66	34	75	25	99.8	0.2
TPD (Kouchi & Yamamoto 1995)	20	29	71	48	52	–	–	–	
TPD (Gudipati et al. 2023)	56	76	24	–	–	69	31	70	30

this to the total CO_2 production per orbit. The result yields that $0.68^{+0.25}_{-0.16}$ per cent of the total CO_2 production may be inherited from the previous apparition in the form of frost. Given that the subsolar latitude is moving farther south afterwards (Fig. 3), additional CO_2-frost may also be released after this point in time. However, its contribution is then hidden in the sublimation of fresh CO_2, which still contains all the trapped species and dominates the outgassing. But also before 2015 February, a fraction of the outgassing CO_2 from the Southern hemisphere may be pristine. Therefore, the provided uncertainty reflects the outgassing of CO_2 frost ending either one month earlier or later (compared to 2015 early-February shown in Fig. 8), respectively.

Despite these uncertainties, frost seems to be an important process involving various species and different time as well as length-scales, that is, volatiles, upon sublimation, may leave the comet or re-freeze on other, colder locations inside the nucleus or on its surface. It is thus also interesting to compare our results to the recent H_2O detection at main belt comet 238P/Read: Kelley et al. (2023) reported a CO_2/H_2O<0.7 per cent. The comet's CO_2-dominated ice phase may thus have been lost over time or its CO_2 activity is quenched. At 67P, we found about 1 per cent CO_2 to be present and associated with H_2O. In order to reduce the minimum amount of CO_2 with respect to H_2O in 67P, the comet would have to undergo water frost cycles that release trapped volatiles similar to the situation discussed for CO_2. In the case of comet 238P/Read, there are temporal changes in the observed H_2O activity: Kelley et al. (2023) reported that devolatilization of the surface takes place on orbital time-scales and the comet's activity is gradually reduced. Frequent H_2O frost cycles may hence have occurred in the past or may even be ongoing.

5.7 The odd case of CO

CO remains poorly understood during the early mission phase. As opposed to the other highly volatile molecules (cf. Section 5.6), the CO density, measured locally at Rosetta, was enhanced and not depleted when the density was reconstructed based on the fractions associated with H_2O and CO_2. Furthermore, when investigating the absolute production rate, CO was first elevated and showed a decreasing activity inbound from >3.5 to ∼2.5 au, even more pronounced than CO_2 (Combi et al. 2020; Läuter et al. 2020).

It is interesting to note that this peculiar behaviour has been observed before, for example, inbound at just about the same heliocentric distance range at comet Hale-Bopp (Biver et al. 2002), another returning comet (Bailey et al. 1996) with strong seasonal outgassing (Kührt 1999) associated with a highly oblique spin axis (Jorda et al. 1997).

The enhanced CO outgassing occurs during the same early time period of alleged CO_2 frost outgassing (cf. Section 5.6). This may indicate a common process, that is, the release of CO frost, which is hence not associated with H_2O and CO_2 and thus underestimated in the reconstructed density. However, this would raise some additional questions, in particular associated with the substantially lower sublimation temperature of CO compared to CO_2 (cf. Table 4). Also CH_4, which has a comparably low sublimation temperature and is co-released in similar proportions with H_2O and CO_2, does not show the same peculiar behaviour or at least to a lesser degree.

Another possibility is irradiation of CO_2 ice which results in the formation of CO, which in turn results in CO trapped in CO_2 and thus follows a strong correlation between the two molecules (Martín-Doménech et al. 2015). But also this explanation has a number of shortcomings. Seasonal carbon dioxide frost has been seen on the surface of the Southern hemisphere of 67P (Filacchione et al. 2016), however, there may be a lot more stored underneath the surface, protected from most photons and energetic particles. Additionally, the Southern hemisphere was in winter during the aphelion period, hence a large fraction of its surface witnessed constant night which limits photolysis and largely protects it from radiolysis by solar wind particles. Furthermore, the heliocentric distance was beyond 4 au for most parts of that phase which leads to low photon and solar wind particle fluxes.

In this discussion, however, we cannot delve into the details associated with the retention of these highly volatile molecules. Clearly, further work is required to understand frost cycles involving different species and the associated diffusion through the porous media of the comet's nucleus including release, re-trapping, and re-freezing processes.

5.8 Future mission outlook

ESA's new F-class mission Comet Interceptor is designed to be the first spacecraft to flyby a DNC, that is, a comet that will enter the inner solar system for the first time (Snodgrass & Jones 2019). Such a target is possibly more pristine compared to the comets visited by spacecraft thus far. CO, for instance, could still be a major (host) species.

Heating and hence loss of highly volatile species through irradiation by the protosun (Davidsson 2021) and by galactic cosmic rays (Gronoff et al. 2020) is altering the outermost tens of metres of objects residing in either the Oort Cloud or the Kuiper Belt (Maggiolo et al. 2020). Additionally, heating by catastrophic collisions (Jutzi & Michel 2020; Davidsson 2023) and radiogenic elements (De Sanctis et al. 2001) may have taken place already. Putting additional

constraints on the degree of these alterations is a major goal of Comet Interceptor. One key measurement of the mission will hence be to obtain relative abundances of highly volatile molecules, such as CO, O_2, and CH_4, for comparison to the ones observed in different families of comets.

Nevertheless, the situation remains complicated, for example, a recent survey has shown that DNCs tend to have lower CO/CO_2 ratios compared to OCCs (Harrington Pinto et al. 2022).

Furthermore, our findings may also be relevant for a cryogenic sample return from the surface of a comet. Since the most likely target for such a mission is a JFC, it is estimated that the ice phases of highly volatile species are lost from at least the surface and outgassing layer of the nucleus.

6 SUMMARY AND CONCLUSIONS

In this paper, we analysed data from the ROSINA mass spectrometer DFMS and pressure sensor COPS, obtained throughout most of the Rosetta mission time, that is, during a period of more than 24 months. The combined measurements provide the local gas density at the location of the Rosetta spacecraft. From this data set, we investigated correlations among different volatile species with regard to the two main ice phases in comet 67P, H_2O and CO_2. A key finding is that the local abundance of the highly volatile molecules, such as CO and CH_4, can be reproduced by a linear combination of the H_2O and CO_2 densities, independent of heliocentric distance, subsolar latitude, and the location of the Rosetta spacecraft. We also showed that a fraction of the CO_2 is likely associated to the outgassing of H_2O. The fitted correlation parameters have been compared to relevant TPD laboratory experiments from the literature. In conclusion, the following key results were obtained:

(i) The results for comet 67P show that highly volatile molecules are simultaneously associated with the two major species, H_2O and CO_2, although the proportions vary depending on the species.

(ii) No ice phase dominated by highly volatile species, which sublimate at temperatures well below 70 K, is required to explain the measured data. A large fraction of these ices have most likely been lost from 67P or they were never part of the comet to begin with. Loss may already occur at even lower temperatures if ample time is available, that is, internal heating up to ∼70 K may not be required to explain the findings at 67P (cf. Parhi & Prialnik 2023). The absence of low temperature ices may also relax the requirements for a cryogenic surface sample return mission to a JFC.

(iii) TPD experiments from the laboratory show similar behaviour as observed at 67P: gases of highly volatile species are trapped in different proportions in or below both H_2O and CO_2 (Kouchi & Yamamoto 1995; Notesco & Bar-Nun 2005; Gudipati et al. 2023). This suggests the inheritance of amorphous ices, which trapped these highly volatile species well before the formation of the solar system. For obvious reasons, TPD experiments often employ a single temperature to freeze out the different species together, for example, 10 K by Kouchi & Yamamoto (1995) and Gudipati et al. (2023). This may not reflect the formation conditions for the ices incorporated into the comet. Also, in these experiments the samples are heated from the bottom, unlike the situation at a comet, where the ices are heated from the top by solar insolation and erosion and thermal skin depths can be comparable close to the sun. Furthermore, other types of ices cannot be excluded, provided similar behaviour can be observed. Additional laboratory and modelling work is required.

(iv) The presented results are also in line with thermal modelling of comets and KBOs, which shows that significant amounts of ices dominated by highly volatile species, such as CO, may have been lost from these small icy bodies (De Sanctis et al. 2001; Parhi & Prialnik 2023). This loss may even be enhanced for a JFC, like 67P, for which internal heating up to 70 K is expected to have taken place during the Centaur stage (Guilbert-Lepoutre et al. 2016). Indeed, when comparing families of comets, somewhat elevated CO/H_2O ratios may be present in OCCs compared to JFCs (A'Hearn et al. 2012). ESA's Comet Interceptor mission, which is designed to visit a DNC, will further shed light on the loss of low temperature ice phases (Snodgrass & Jones 2019), keeping in mind that also DNCs may have their surface layer substantially processed before reaching the inner solar system (De Sanctis et al. 2001; Maggiolo et al. 2020; Harrington Pinto et al. 2022; Davidsson 2023).

(v) The exact amounts of CH_4, CO, O_2, N_2, etc. that were lost due to thermal and collisional heating (Jutzi & Michel 2020; Davidsson et al. 2021; Davidsson 2023; Parhi & Prialnik 2023), furthermore, depend on the original trapping temperature of the ices incorporated into the comet. Due to the evolutionary loss of the ice phases dominated by highly volatile species, it is very challenging to recover this temperature. A single temperature at which all species freeze out together is unlikely.

(vi) Data obtained early in the mission are distinctly different. This was a time when the H_2O outgassing was dominated by the evolutionary processed Northern hemisphere but CO_2 originated from the south. Our results indicate that H_2O kept CO_2 and highly volatile molecules such as CH_4, C_2H_6, C_3H_8, O_2, and H_2S trapped, even if transported as icy grains from the Southern to the Northern hemisphere where the water sublimation then occurred. The CO_2-dominated phase, on the other hand, was lost from such grains. This is in line with numerical simulations by Davidsson et al. (2021).

(vii) CO_2 outgassing during the early mission phase was observed predominantly from the Southern hemisphere which was in winter during that time. Our results indicate that the CO_2 measured during that time was processed. A possible explanation is seasonal frost, that is, CO_2, which sublimated during the outbound journey of the previous apparition but refroze before leaving the nucleus. In this process, the trapped (highly) volatiles may have been lost. Seasonal CO_2 frost has indeed been observed on the surface of 67P's Southern hemisphere (Filacchione et al. 2016). We derive an order of magnitude of the seasonally inherited amount of CO_2 frost of one per cent relative to the total CO_2 outgassing.

(viii) As opposed to the molecules discussed above, the CO abundance was elevated early in the mission. This remains poorly understood because other highly volatile molecules, with comparable sublimation temperatures, exhibit the opposite behaviour. For instance, CH_4 was depleted in CO_2 during the same time period. Interestingly, similarly elevated CO activity, at comparable heliocentric distances during the inbound part of the orbit, has already been observed at comet Hale-Bopp (Biver et al. 2002). Seasonal CO frost, carried over from the last orbit similar to CO_2, would be able to explain these observations. The low temperature required to freeze out CO, however, counters that argument.

(ix) Additional laboratory experiments are required. It is key that these experiments include both H_2O and CO_2 in variable proportions, together with the species to be studied, for example, N_2, CO, CH_4, etc. The relative proportions of the latter should be similar to the ones found in comets (e.g. 67P in Table 4), with highly volatile species being present in trace amounts, maybe somewhat enhanced to account for the loss of the low-temperature ices over the lifetime of the comet (cf. Table 5). We do not know the detailed formation of the main ices incorporated in the nucleus. If the

H_2O and CO_2 ices formed separately, for instance in a layered mantle, similar to the so-called Greenberg (1982) particles, then the trapping (or chemical formation) of trace species may be subject to vastly varying CO_2/H_2O ratios. Laboratory measurements should therefore also cover CO_2/H_2O ratios that are higher than what is commonly observed in comets. Furthermore, measurements with varying trapping temperatures are required to investigate whether the formation temperature of the comet can be recovered from the relative partitioning of highly volatile species in H_2O and CO_2 ices, given that the ice-phases dominated by highly volatile species will be mostly lost afterwards. Last but not least, also frost cycles of H_2O, CO_2, and possibly CO ices containing impurities ought to be investigated further.

ACKNOWLEDGEMENTS

We gratefully acknowledge the work of the many engineers, technicians and scientists involved in the Rosetta mission and in the ROSINA (Rosetta Orbiter Spectrometer for Ion and Neutral Analysis) instrument in particular. Without their contributions, ROSINA would not have produced such outstanding results. Rosetta is an European Space Agency (ESA) mission with contributions from its member states and the National Aeronautics and Space Administration (NASA). Work by MR, NH, and DRM was funded by the Canton of Bern and the Swiss National Science Foundation (SNSF; 200020_207312). MRC and YS were funded by NASA grants 80NSSC18K1280 and 80NSSC22K1064, respectively. MSG thanks NASA's Discovery Data Analysis Program (DDAP) for funding and his part of the work was carried out at the Jet Propulsion Laboratory, California Institute of Technology, under a contract with NASA (80NM0018D0004). NFWL and KAK acknowledge support from SNSF Ambizione grant 193453 and NCCR PlanetS. SFW acknowledges the financial support of the SNSF Eccellenza Professorial Fellowship (PCEFP2_181150).

We thank the referee, Gianrico Filacchione, for the constructive feedback that enabled us to significantly improve the quality of our manuscript.

DATA AVAILABILITY

All Rosetta/ROSINA data are available through the NASA Planetary Data System (PDS) and ESA's Planetary Science Archive (PSA).

REFERENCES

A'Hearn M. F. et al., 2011, Science, 332, 1396
A'Hearn M. F. et al., 2012, ApJ, 758, 29
Almayrac M. G., Bekaert D. V., Broadley M. W., Byrne D. J., Piani L., Marty B., 2022, Plan. Sci. J., 3, 252
Altwegg K. et al., 2015, Science, 347, 1261952
Altwegg K. et al., 2017a, Phil. Trans. R. Soc. A, 375, 20160253
Altwegg K. et al., 2017b, MNRAS, 469, S130
Altwegg K., Balsiger H., Fuselier S. A., 2019, ARA&A, 57, 113
Altwegg K. et al., 2020, Nat. Astron., 4, 533
Anderson S. E., Rousselot P., Noyelles B., Jehin E., Mousis O., 2023, MNRAS, 524, 5182
Bailey M. E., Emel'yanenko V. V., Hahn G., Harris N. W., Hughes K. A., Muinonen K., Scotti J. V., 1996, MNRAS, 281, 916
Balsiger H. et al., 2007, Space Sci. Rev., 128, 745
Balsiger H. et al., 2015, Sci. Adv., 1, e1500377
Bar-Nun A., Notesco G., Owen T., 2007, Icarus, 190, 655
Behmard A., Fayolle E. C., Graninger D. M., Bergner J. B., Martín-Doménech R., Maksyutenko P., Rajappan M., Öberg K. I., 2019, ApJ, 875, 73
Bieler A. et al., 2015, Nature, 526, 678
Biver N., Bockelée-Morvan D., 2019, ACS Earth Space Chem., 3, 1550
Biver N. et al., 2002, in Cometary Science after Hale-Bopp. Springer, New York, p. 5
Biver N. et al., 2019, A&A, 630, A19
Bockelée-Morvan D., Crovisier J., Mumma M. J., Weaver H. A., 2004, in Festou M. C., Keller H. U., Weaver H. A., eds, Comets II. Univ. Arizona Press, Tucson, AZ, p. 391
Bockelée-Morvan D. et al., 2015, A&A, 583, A6
Bockelée-Morvan D. et al., 2016, MNRAS, 462, S170
Boogert A. A., Gerakines P. A., Whittet D. C., 2015, ARA&A, 53, 541
Burke D. J., Brown W. A., 2010, Phys. Chem. Chem. Phys., 12, 5947
Burke D. J., Brown W. A., 2015, MNRAS, 448, 1807
Cheng Y. C. et al., 2022, A&A, 663, 17
Ciarniello M. et al., 2022, Nat. Astron., 6, 546
Collings M. P., Anderson M. A., Chen R., Dever J. W., Viti S., Williams D. A., McCoustra M. R., 2004, MNRAS, 354, 1133
Combi M. R., Tenishev V. M., Rubin M., Fougere N., Gombosi T. I., 2012, ApJ, 749, 29
Combi M. et al., 2020, Icarus, 335, 113421
Crovisier J., Biver N., Bockelee-Morvan D., Colom P., Jorda L., Lellouch E., Paubert G., Despois D., 1995, Icarus, 115, 213
Davidsson B. J. R., 2021, MNRAS, 505, 5654
Davidsson B. J. R., 2023, MNRAS, 521, 2484
Davidsson B. J. et al., 2021, Icarus, 354, 114004
De Sanctis M. C., Capria M. T., Coradini A., 2001, AJ, 121, 2792
De Sanctis M. C. et al., 2015, Nature, 525, 500
Dello Russo N., Kawakita H., Vervack R. J., Weaver H. A., 2016, Icarus, 278, 301
Eberhardt P., 1999, in Altwegg K., Ehrenfreund P., Geiss J., Huebner W. F., eds, Composition and Origin of Cometary Materials. Springer, Dordrecht, p. 45
El-Maarry M. R. et al., 2015, A&A, 583, A26
Faggi S., Villanueva G. L., Mumma M. J., Paganini L., 2018, ApJ, 156, 68
Filacchione G. et al., 2016, Science, 354, 1563
Filacchione G. et al., 2020, Nature, 578, 49
Fray N., Schmitt B., 2009, Planet. Space Sci., 57, 2053
Fulle M., Altobelli N., Buratti B., Choukroun M., Fulchignoni M., Grün E., Taylor M. G. G. T., Weissman P., 2016, MNRAS, 462, S2
Gasc S. et al., 2017, MNRAS, 469, S108
Geiss J., 1988, in Exploration of Halley's Comet. Springer-Verlag, Berlin, p. 859
Glassmeier K.-H., Boehnhardt H., Koschny D., Kührt E., Richter I., 2007, Space Sci. Rev., 128, 1
Gomes R., Levison H. F., Tsiganis K., Morbidelli A., 2005, Nature, 435, 466
Graf S. et al., 2004, J. Geophys. Res., 109, E07S08
Greenberg J. M., 1982, What are Comets Made of? A Model based on Interstellar Dust. Univ. Arizona Press, Tucson, AZ, p. 131
Gronoff G. et al., 2020, ApJ, 890, 89
Groussin O. et al., 2019, Space Sci. Rev., 215, 29
Gudipati M., Fleury B., Wagner R., Henderson B. L., Altwegg K., Rubin M., 2023, Faraday Discuss. 245, 467
Guilbert-Lepoutre A., Rosenberg E. D., Prialnik D., Besse S., 2016, MNRAS, 462, S146
Gulkis S. et al., 2015, Science, 347, aaa0709
Hänni N., Altwegg K., Combi M., Fuselier S. A., De Keyser J., Rubin M., Wampfler S. F., 2022, Nat. Comm., 13, 3639
Hansen K. C. et al., 2016, MNRAS, 462, S491
Harrington Pinto O., Womack M., Fernandez Y., Bauer J., 2022, Plan. Sci. J., 3, 247
Hässig M. et al., 2015, Science, 347, aaa0276
Herbst E., Van Dishoeck E. F., 2009, ARA&A, 47, 427
Jorda L., Rembor K., Lecacheux J., Colom P., Colas F., Frappa E., Lara L. M., 1997, Earth Moon Planets, 77, 167
Jutzi M., Asphaug E., 2015, Science, 348, 1355
Jutzi M., Michel P., 2020, Icarus, 350, 113867
Keller H. U. et al., 2015, A&A, 583, A34
Keller H. U. et al., 2017, MNRAS, 469, S357

Kelley M. S. P., Hsieh H. H., Bodewits D., Saki M., Villanueva G. L., Milam S. N., Hammel H. B., 2023, Nature, 619, 720
Kouchi A., Kuroda T., 1990, in ESA SP-315: Formation of Stars and Planets, and the Evolution of the Solar System. ESA, Noordwijk, p. 193
Kouchi A., Sirono S.-i., 2001, Geophys. Res. Lett., 28, 827
Kouchi A., Yamamoto T., 1995, Progress in Crystal Growth and Character. Mater., 30, 83
Kramer T., Läuter M., Rubin M., Altwegg K., 2017, MNRAS, 469, S20
Kramer T., Läuter M., Hviid S., Jorda L., Keller H. U., Kührt E., 2019, A&A, 630, A3
Kührt E., 1999, Space Sci. Rev., 90, 75
Lamberts T., Ioppolo S., Cuppen H. M., Fedoseev G., Linnartz H., 2015, MNRAS, 448, 3820
Laufer D., Bar-Nun A., Ninio Greenberg A., 2017, MNRAS, 469, S818
Läuter M., Kramer T., Rubin M., Altwegg K., 2019, MNRAS, 483, 852
Läuter M., Kramer T., Rubin M., Altwegg K., 2020, MNRAS, 498, 3995
Le Roy L. et al., 2015, A&A, 583, A1
Ligterink N. F. W., Minissale M., 2023, A&A, 676, A80
Ligterink N. F. W., Walsh C., Bhuin R. G., Vissapragada S., Terwisscha van Scheltinga J., Linnartz H., 2018, A&A, 612, A88
Luspay-Kuti A. et al., 2015, A&A, 583, A4
Luspay-Kuti A. et al., 2016, Sci. Adv., 2, e1501781
Luspay-Kuti A. et al., 2019, A&A, 630, A30
Luspay-Kuti A. et al., 2022, Nat. Astron., 6, 724
Maggiolo R. et al., 2020, ApJ, 901, 136
Maquet L., 2015, A&A, 579, A78
Marshall D. W. et al., 2017, A&A, 603, A87
Martín-Doménech R., Muñoz Caro G. M., Bueno J., Goesmann F., 2014, A&A, 564, A8
Martín-Doménech R., Manzano-Santamaría J., Muñoz Caro G. M., Cruz-Díaz G. A., Chen Y. J., Herrero V. J., Tanarro I., 2015, A&A, 584, A14
Marty B. et al., 2017, Science, 356, 1069
Massironi M. et al., 2015, Nature, 526, 402
Minissale M. et al., 2022, ACS Earth Space Chem., 6, 597
Mousis O. et al., 2017, ApJ, 839, L4
Mousis O. et al., 2018, ApJ, 865, L11
Nevejans D., Neefs E., Kavadias S., Merken P., Van Hoof C., 2002, Int. J. Mass Spec., 215, 77
Notesco G., Bar-Nun A., 2005, Icarus, 175, 546
Opitom C. et al., 2019, A&A, 624, A64
Parhi A., Prialnik D., 2023, MNRAS, 522, 2081
Rubin M., Fougere N., Altwegg K., Combi M. R., Roy L. L., Tenishev V. M., Thomas N., 2014, ApJ, 788, 168
Rubin M. et al., 2015, Science, 348, 232
Rubin M. et al., 2018, Science Adv., 4, eaar6297
Rubin M., Bekaert D. V., Broadley M. W., Drozdovskaya M. N., Wampfler S. F., 2019a, ACS Earth Space Chem., 3, 1792
Rubin M. et al., 2019b, MNRAS, 489, 594
Rubin M., Engrand C., Snodgrass C., Weissman P., Altwegg K., Busemann H., Morbidelli A., Mumma M., 2020, Space Sci. Rev., 216, 1
Sarid G., Volk K., Steckloff J. K., Harris W., Womack M., Woodney L. M., 2019, ApJ, 883, L25
Schroeder I. R. et al., 2019, MNRAS, 489, 4734
Schuhmann M. et al., 2019, A&A, 630, A31
Shinnaka Y., Kawakita H., Jehin E., Decock A., Hutsemékers D., Manfroid J., 2016, MNRAS, 462, S124
Sierks H. et al., 2015, Science, 347, aaa1044
Simon A., Öberg K. I., Rajappan M., Maksiutenko P., 2019, ApJ, 883, 21
Smith R. S., Huang C., Wong E. K. L., Kay B. D., 1997, Phys. Rev. Lett., 79, 909
Snodgrass C., Jones G. H., 2019, Nat. Comm., 10, 1
Taquet V., Furuya K., Walsh C., van Dishoeck E. F., 2016, MNRAS, 462, S99
Taylor M., Altobelli N., Buratti B., Choukroun M., 2017, Phil. Trans. R. Soc. A Sci., 375, 20160262
Tenishev V., Combi M., Davidsson B., 2008, ApJ, 685, 659
Thomas N. et al., 2015, A&A, 583, A17
Thomas N. et al., 2019, Space Sci. Rev., 215, 1
Tosi F. et al., 2019, Nat. Astron., 3, 649
Weissman P., Morbidelli A., Davidsson B., Blum J., 2020, Space Sci. Rev., 216, 1
Zamirri L., Casassa S., Rimola A., Segado-Centellas M., Ceccarelli C., Ugliengo P., 2018, MNRAS, 480, 1427

APPENDIX A: DETAILS ON ROSINA DFMS AND COPS

ROSINA was composed of three instruments (Balsiger et al. 2007), the DFMS, the Reflectron-type Time-of-Flight mass spectrometer, and the COPS. All three sensors were operated through the Data Processing Unit. The data used in this work are based on the combination of relative gas abundances measured with DFMS and the total gas densities obtained with COPS. Both sensors are described briefly in following.

COPS contained two pressure gauges out of which the Nude Gauge (NG) forms the baseline of this work. The NG was an extractor-type ionization gauge, designed to measure the local gas density surrounding the Rosetta spacecraft. Neutral gas was bombarded by 150 eV electrons inside an open ionization volume surrounded by grids to trap ionizing electrons and guiding freshly formed ions towards the collector electrode. Both grids were very coarse to minimize interaction with the cometary neutral gas flow. At the collector electrode, the current of ions was measured by a highly sensitive electrometer. The ratio of the measured ion current to the regulated electron emission current, nominally set to 100 μA, is proportional to the neutral gas density inside the ionization volume after applying the lab-calibrated instrument sensitivity factors (Graf et al. 2004).

The DFMS was a mass spectrometer in Nier–Johnson design with a mass resolution of $m/\Delta m = 3000$ for the full width at 1 per cent peak height on mass/charge 28 $u\,e^{-1}$. Neutral gas entering the ion source was ionized by 45 eV electrons from a hot filament emitting a current of 200 μA. The newly formed ions were accelerated and then deflected first by 90° in an electrostatic analyser and then by 60° in the field of a permanent magnet. The offset potential of the ion source ensured that external coma ions would not have a suitable energy to pass through this analyser section. Afterwards, suitable quadrupole electric fields widened up the ion beam, which was hence further separated by mass/charge, onto the Micro Channel Plates (MCP) located on top of a position-sensitive Linear Electron Detector Array (LEDA) with two parallel rows of 512 pixels each (Nevejans et al. 2002).

For a selected set of ion optical potentials only a limited mass/charge range, distributed across the pixels, could be measured (e.g. $\pm 0.25\,u\,e^{-1}$ at 28 $u\,e^{-1}$). Therefore, the voltages in DFMS had to be adjusted for each mass/charge to be measured. Obtaining a single spectrum took about 30 s, which included some 10 s for setting and settling of the voltages followed by 20 s of signal integration. A mass scan covering each integer mass/charge from 13 to 100 $u\,e^{-1}$ therefore lasted about 45 min.

If peaks in the MCP/LEDA spectra were overlapping due to close mass/charge, each peak was fitted by the sum of two Gaussians, one about 10 per cent of the amplitude of the other but 2–3 times wider. One example is N_2 which is found close to CO, the former a minor volatile and the latter a major cometary parent species (Rubin et al. 2015). Furthermore, since DFMS measured the mass lines in sequence, the obtained signals of the individual species were linearly interpolated in time such that ratios of different volatile species could be derived.

The ionization process did not only produce parent ions but also break up the molecules. These so-called fragmentation patterns depend on the molecule and the energy of the ionizing electron and had to be taken into account when deriving relative abundances. This includes the subtraction of the signal from higher mass parent molecules, for example, the electron impact dissociation contribution from $CO_2 + e^- \rightarrow CO^+ + O + 2e^-$ had to be subtracted from the measured CO^+ signal. Once fragmentation has been taken care of, the species-dependent sensitivity factors were applied, taking into account that the detector was operated in analogue mode and had hence a different yield for incident ions. Furthermore, also the transmission through the instrument and the ionization cross-section differed among the molecules. Finally, the relative abundances of the coma gases were obtained and, by scaling to the total density measured with COPS, the absolute densities of these species were retrieved. More details on these measurements, how they have been processed, and the associated calibration factors can be found in Rubin et al. (2019b).

APPENDIX B: FIGURE COLLECTION OF OTHER HIGHLY VOLATILE MOLECULES

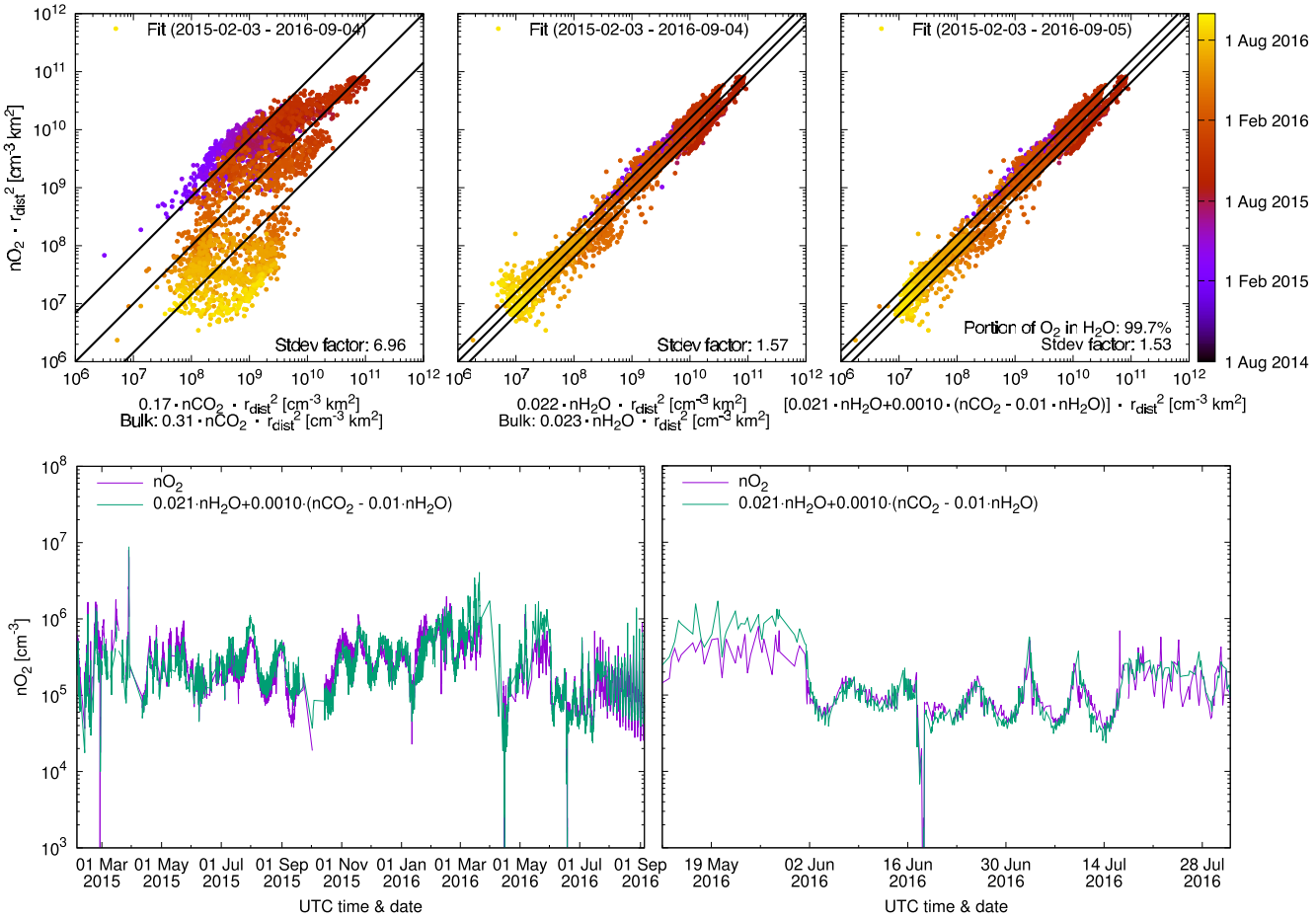

Figure B1. Same as Fig. 4, but for O_2 instead of CH_4.

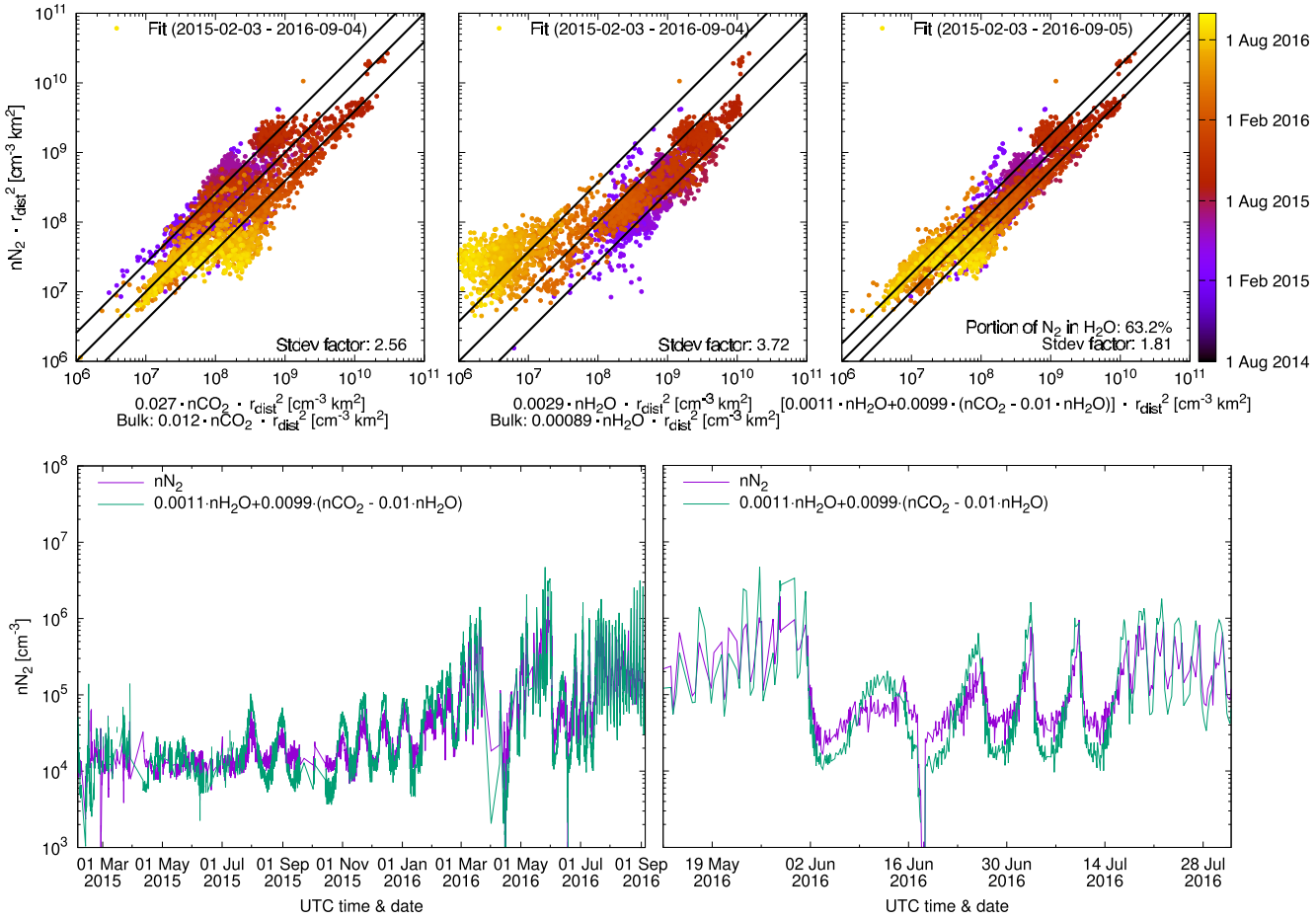

Figure B2. Same as Fig. 4, but for N_2 instead of CH_4.

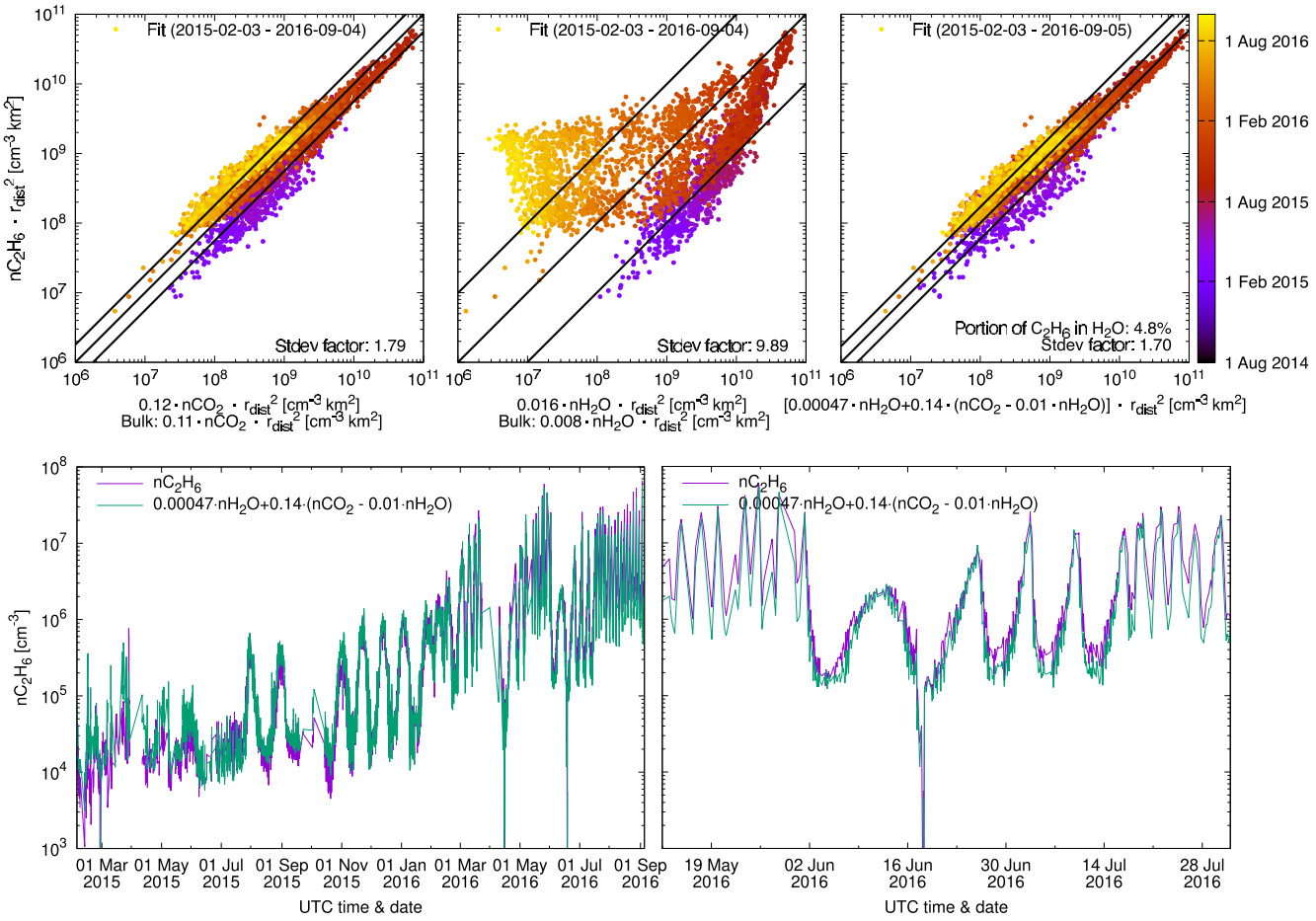

Figure B3. Same as Fig. 4, but for C_2H_6 instead of CH_4.

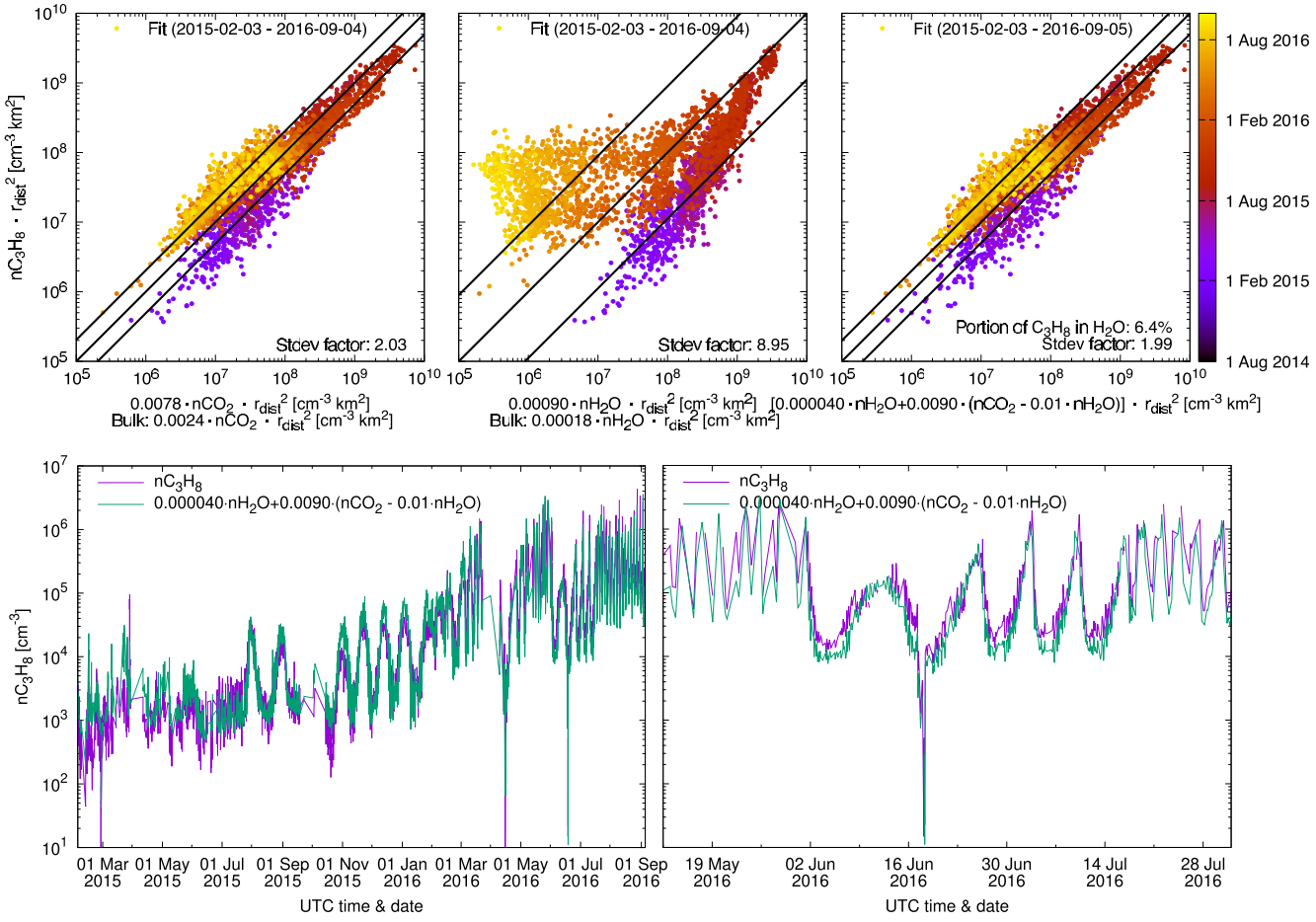

Figure B4. Same as Fig. 4, but for C_3H_8 instead of CH_4.

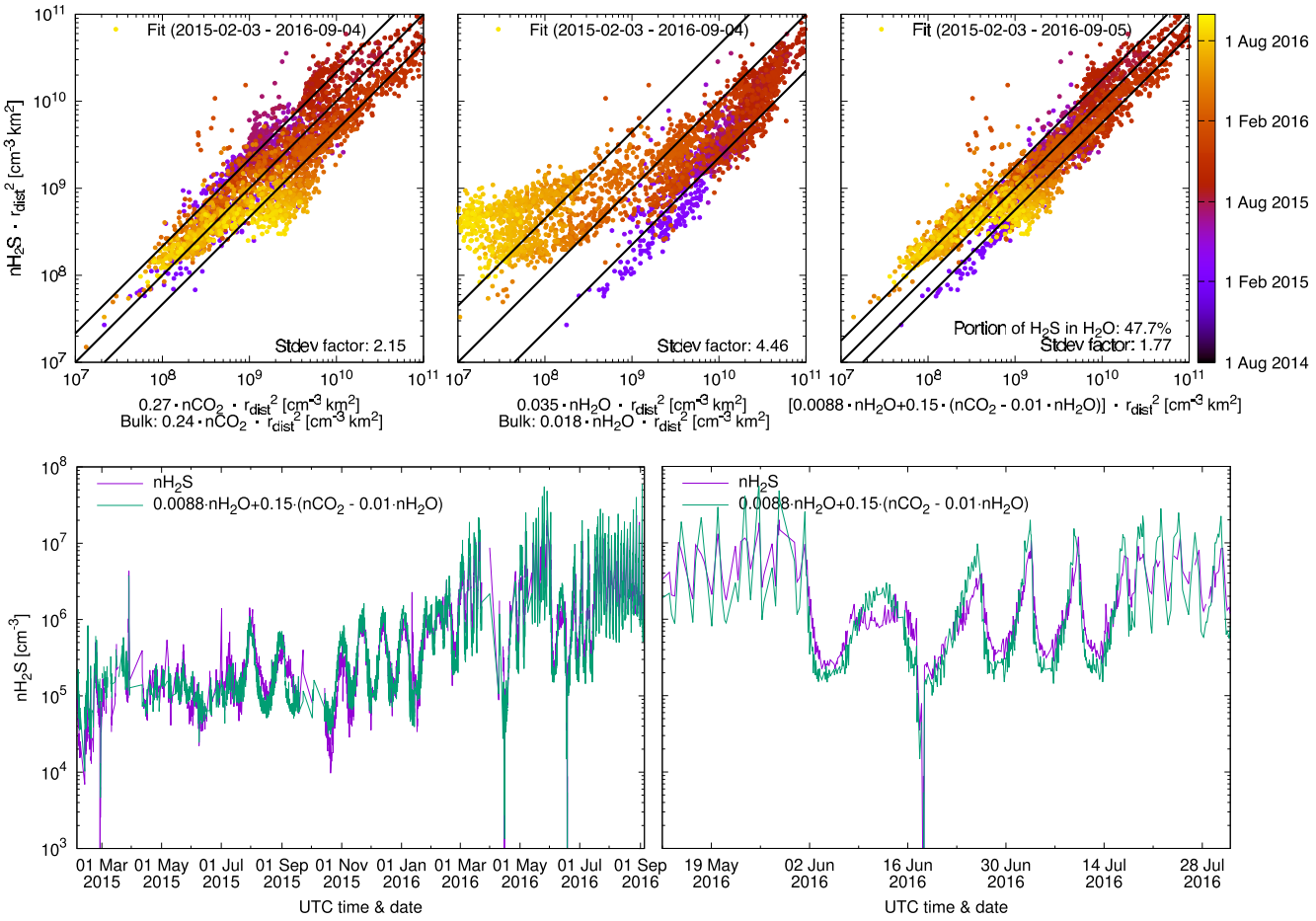

Figure B5. Same as Fig. 4, but for H_2S instead of CH_4.

This paper has been typeset from a TEX/LATEX file prepared by the author.